Higgs inflation with nonminimal couplings

Yukari Nakanishi*

February 20, 2018

Abstract

The Higgs field is the only scalar field in the Standard Model of particle physics. Because the potential shape of the Standard Model Higgs is not suitable for the inflation, the nonminimal coupling between Higgs and the Ricci scalar is necessary to use the Higgs field as an inflaton. In this thesis, we employ two approaches on Higgs inflation model with general nonminimal couplings. First we consider the prescription dependence of the Higgs effective potential. It has been considered that the prescriptions correspond to the choice of frame in which a field-independent ultraviolet cutoff is defined. We have shown that the difference between prescriptions comes from the choice of counterterm to cancel the logarithmic divergence in the counterterm formalism. We also point out that the difference can be absorbed into the choice of tree-level potential from the infinitely possibilities, including higher-dimensional terms. Second, we assume that a low-energy effective theory is valid below a certain energy scale and that the slow-roll inflation occurred above the cutoff scale. We obtain the lower bound on the tensor-to-scalar ratio r even if we do not know the theory at high-energy scales. We consider the Higgs-portal Z_2 dark-matter model as an example, and we calculate the lower bound on the tensor-to-scalar ratio r and the upper bound on the dark-matter mass $m_{\rm DM}$. We obtain $r \gtrsim 4 \times 10^{-2}$ and $m_{\rm DM} \lesssim 1.1\,\text{TeV}$ in absence of heavy right-handed neutrinos. When there is contribution from heavy right-handed neutrinos, the most conservative bound becomes $r \gtrsim 10^{-5}$ and $m_{\rm DM} \lesssim 1.6\,\text{TeV}$.

*nakanishi@het.phys.sci.osaka-u.ac.jp

Contents

Acknowledgements

I would like to express my gratitude to my collaborators, Kin-ya Oda, Prof. Hikaru Kawai and Yuta Hamada. I also thank Prof. Takahiro Kubota, Prof. Kentaro Nagamine, Minoru Tanaka, Tomohiro Abe, Xiangdong Ji, Kiyoharu Kawana, Jinsu Kim, Tae Geun Kim, Seong Chan Park, Stanislav Rusak, Mikhail Shaposhnikov, and Satoshi Yamaguchi for useful discussions and comments. Finally, I thank all members of Particle Physics Theory Group at Osaka University, especially my supervisors Prof. Yutaka Hosotani and Prof. Shinya Kanemura, for efforts to keep good research environment.

Publications

This thesis is based on following two papers.

- *Meaning of the field dependence of the renormalization scale in Higgs inflation*
  Yuta Hamada, Hikaru Kawai, Yukari Nakanishi, and Kin-ya Oda
  Phys. Rev. D **95**, 103524 [arXiv:1610.05885 [hep-th]]

- *Higgs inflation puts lower and upper bounds on tensor-to-scalar ratio and on Higgs-portal-dark-matter mass*
  Yuta Hamada, Hikaru Kawai, Yukari Nakanishi, and Kin-ya Oda
  [arXiv:1709.09350 [hep-th]]

1 Introduction

The Big Bang theory is a successful model in cosmology. It can explain the universe history after the Big Bang nucleosynthesis, however, we have still some unsolved problems: our universe has unnaturally small curvature and homogeneous energy distribution. The inflationary paradigm [1, 2, 3, 4] is one of approaches to solve such cosmological problems. An epoch inflation when the universe expanded rapidly in the early time makes the spatial curvature small. It shrinks the comoving distance, which represents the distance that two points can interact within finite time, and also makes the homogeneous universe possible. The inflation also dilutes the (number or energy) density of particles and structures that existed before it, hence we may understand the nonexistence of things such as monopoles.

Then, what is the mechanism of inflation? There are many possibilities proposed from the point of view of particle physics and gravitational theory. However, at present, we do not know which model is the truth. In recent decades, the observations also have been developed and we obtained some information about the inflation. Direct detection of photons is the most reliable method in the investigation of the history of universe. Though the direct observation of inflation is difficult, we can observe the last scattered photons called cosmic microwave background (CMB), and its temperature perturbation and polarization tell us many properties of the inflation. An important observable is the tensor-to-scalar ratio r which is the ratio of amplitude of tensor and scalar perturbations. In principle, the tensor perturbation can be observed as the primordial gravitational waves. Recently there is a report of detecting the signal of gravitational wave from binary black holes [5]. However, the detection of primordial gravitational wave is rather difficult and we may only observe it indirectly via the B-mode of CMB polarization at present. The upper bound on the tensor-to-scalar ratio obtained by Planck is $r \leq 0.09$ within 2σ C.L. [6]. Another observable parameter is the spectral index n_s of the power spectrum of the scalar perturbation, and it is constrained $n_s = 0.968 \pm 0.006$ within 1σ C.L. [6]; we will give a detailed review in Sec. 2.

The field which causes the inflation is called inflaton. The matter nor radiation component in the universe cannot induce the inflation because their pressure is positive and they always shrink the space. On the other hand, scalar fields can become candidates for inflaton. The Standard Model (SM) of particle physics has the Higgs field as the only scalar field which has been discovered [7, 8]. Although the pure SM Higgs cannot reproduce the observed values of r and n_s, we can make suitable models by introducing fewer assumptions on the SM than with other undiscovered scalar particles. In this thesis, we concentrate on the Higgs inflation model and consider issues on it.

A simple extension is to add nonminimal couplings between the Higgs field φ and the Ricci scalar R. By switching frames by conformal transformation, we obtain the suitable shape of Higgs potential for the inflation [9, 10]. This model predicts parameters of the

closest to the best fit point in the r-n_s plane among various inflation models [11]. In classical theory, there is no problem on such conformal transformation of metric. However, the frame dependence (or independence) of the quantum theory has long been disputed; see e.g. [12, 13, 14, 15, 16, 17, 18, 19].

We often consider the running of couplings in the quantum field theory. When we analyze the nonminimal model, the corrections from the nonminimal couplings appears in general. Under the existence of nonminimal coupling term, it has been said that there are two different "prescriptions" to approximate the renormalized Higgs potential to the tree-level one [20, 21, 22]. A prescription is claimed to correspond to a field-independent[1] ultraviolet cutoff in a specific frame [20, 21], and the different choice of prescription comes down to the different size of the nonminimal coupling for realistic inflation [23, 24]. However, if we start from the identical Lagrangian, it is curious that the field dependence of the cutoff scale changes the result.

In this thesis, we show that we can guarantee the frame independence of the effective action with proper definition of path integral measure and with renormalization condition. We also revisit the relation between the ultraviolet cutoff and the renormalization scale, and clarify that the different choice of the cutoff does not directly relate to the difference prescriptions: it is related to the choice of the counterterm to cancel the logarithmic divergence. We also explain that the difference can be absorbed into the choice of the tree-level potential, including higher-dimensional terms.

On the other hand, the observed value of the Higgs mass $125.09 \pm 0.24\,\mathrm{GeV}$ [25] indicates that the Higgs potential in the SM becomes small and nearly flat by the fermion-loop corrections when the Higgs-field value is close to the Planck-scale; see e.g. Refs. [26, 27, 28, 29, 30, 31, 32, 33, 34, 35, 36, 37, 38]. This is required by the multiple-point principle (MPP) [39, 40, 41, 42]. The inflation model using this flatness at the high-energy scale is called Critical Higgs Inflation [23, 43, 44, 24]. The usual Higgs inflation needs large nonminimal coupling $\sim 10^4$, but the Critical Higgs Inflation does not need so large nonminimal couplings.

The nonminimal coupling reduces the range of scale where the low-energy effective theory is valid. If the nonminimal coupling is sufficiently small, the cutoff scale[2] of the effective theory is close to the Plank scale, and the energy scale at which the inflation occurred becomes high. In this thesis, we show that we can obtain the lower bound on the tensor-to-scalar ratio r even if we do not know the high-energy-scale physics. We consider a specific model of Higgs inflation and analyze the lower bound. Consequently, we find that the lower bound on r which may be tested in the near future.

This thesis is organized as follows. In Sec. 2, we briefly review the slow-roll inflation

[1] In the case of Higgs inflation, the field is Higgs.

[2] This cutoff scale is different from the ones in the discussion of prescriptions: here it means the upper limit of the valid range of the low-energy effective theory.

mechanism and the nonminimal inflation model. In Sec. 3, the first topic of this thesis, the frame (in)dependence and the prescriptions, is discussed. In Sec. 4, we turn to the case of inflation at high-energy scale, and calculate the lower bound on the tensor-to-scalar ratio. Finally in Sec. 5 we give a summary of this thesis.

Throughout this paper, the units of $c = \hbar = 1$ is taken unless otherwise stated.

2 Introduction to Inflation

Single-field models are considered as one of simple possible realization for the inflation. Especially, slow-roll mechanism can produce small tensor-to-scalar ratio, which fits the observations. In this section, the mechanism of single-field slow-roll model is explained.

2.1 Cosmological perturbation theory

First we review the classical cosmology. The homogeneous isotropic background metric (Friedmann-Lemaître-Robertson-Walker metric) is

$$\mathrm{d}s^2 = \mathrm{d}t^2 - a^2(t)\,\mathrm{d}\mathbf{x}^2 \tag{1}$$

where $a(t)$ is a scale factor of the universe.[3] The dynamics of $a(t)$ is calculated from the Einstein equation

$$R_{\mu\nu} - \frac{1}{2}Rg_{\mu\nu} + \Lambda_c g_{\mu\nu} = 8\pi T_{\mu\nu} \tag{2}$$

where Λ_c is the cosmological constant and $T_{\mu\nu}$ is energy-momentum tensor for all components in the universe other than the cosmological constant. From the homogeneity and isotropicity, $T_{\mu\nu}$ has only diagonal components at zeroth order of perturbation,

$$T^{\mu}_{\ \nu} = \begin{pmatrix} -\rho & 0 & 0 & 0 \\ 0 & P & 0 & 0 \\ 0 & 0 & P & 0 \\ 0 & 0 & 0 & P \end{pmatrix} \tag{3}$$

where ρ is the energy density and P is corresponds to pressure. From Eqs. (2) and (3), we obtain the Friedmann equations:

$$\left(\frac{\dot{a}}{a}\right)^2 = \frac{8\pi G}{3}\rho + \frac{\Lambda_c}{3}, \qquad \frac{\ddot{a}}{a} = -\frac{4\pi G}{3}(\rho + 3P) + \frac{\Lambda_c}{3}. \tag{4}$$

The energy components other than the one that causes the inflation can be disregarded during the inflation. If the accelerated expansion had been induced by the cosmological

[3] Throughout this thesis, we ignore the spatial curvature K of the universe because it becomes small during the inflation. We may recover it by $\mathrm{d}\mathbf{x}^2 \to \mathrm{d}\mathbf{x}^2 + K\frac{(\mathbf{x}\cdot\mathrm{d}\mathbf{x})^2}{1-K\mathbf{x}^2}$. Actually the achievement of small curvature $|\Omega_K| < 0.005$ [6] is one of the motivation of the inflation paradigm, as mensioned in the introduction.

constant, the Einstein equation can be easily solved and we obtain $a(t) \propto \exp\Big(\sqrt{\Lambda_c/3}\, t\Big)$. In this case, the Hubble parameter defined as

$$H := \frac{\dot{a}}{a} \tag{5}$$

becomes a constant.

We also define the e-folding number N which stands for how large the universe has expanded during the inflation as

$$N := \ln \frac{a_{\rm end}}{a_{\rm start}}. \tag{6}$$

The observable fluctuations of CMB corresponds to the primordial perturbations at $N =$ 40–60 and it depends on which reheating model we take [45].

Scalar perturbation Next we consider the first-order perturbation theory. Using the gauge-invariant comoving curvature perturbation $\mathcal{R}(t, \mathbf{x})$, the metric is written as

$$\mathrm{d}s^2 = \mathrm{d}t^2 - a^2(t)\, e^{2\mathcal{R}} \mathrm{d}\mathbf{x}^2 \tag{7}$$

in the comoving gauge.

The quantum variable $\mathcal{R}$ obeys a canonical commutation relation with an appropriate normalization. Then the two-point function of the comoving curvature perturbation gives its power spectrum $P_{\mathcal{R}}$ as[4]

$$\langle \mathcal{R}_{\mathbf{k}} \mathcal{R}_{\mathbf{k}'} \rangle = \delta\big(\mathbf{k} + \mathbf{k}'\big)\, P_{\mathcal{R}}(k)\,. \tag{8}$$

Naively, the amplitude of the scalar perturbation $\big\langle \mathcal{R}^2(t, \mathbf{x}) \big\rangle$ is directly connected the temperature perturbation of CMB. From Eq. (8),

$$\big\langle \mathcal{R}^2(t, \mathbf{x}) \big\rangle = \int \frac{\mathrm{d}k}{k} \frac{k^3}{2\pi^2} P_{\mathcal{R}}(k) \tag{9}$$

and the integrand

$$\Delta^2_{\mathcal{R}} := \frac{k^3}{2\pi^2} P_{\mathcal{R}}(k) \tag{10}$$

is the dimensionless power spectrum. The amplitude at the horizon crossing time becomes

$$A_s := \Delta^2_{\mathcal{R}}\big|_{k=aH} = \frac{1}{8\pi^2} \frac{H^2}{M_{\rm P}^2} \frac{1}{\epsilon}\bigg|_{k=aH} \tag{11}$$

[4]We ignore the difference between the comoving curvature perturbation and the curvature perturbation on uniform-density hypersurfaces because the difference disappears on superhorizon scales or under the slow-roll approximation [45]. For the details of the calculation, see also the author's master thesis [46].

where $\epsilon := -\dot{H}/H^2$ is the first Hubble flow function.[5] And we define the spectral index

$$n_s := \frac{\mathrm{d}\ln\Delta^2_{\mathcal{R}}}{\mathrm{d}\ln k} + 1. \tag{12}$$

If the inflation is derived by the cosmological constant, it is known that the dimensionless power spectrum of CMB becomes Harrison-Zel'dovich spectrum [47, 48] which is scale invariant: $n_s = 1$.

Tensor perturbation The metric has also the vector and tensor modes of perturbations. It is known that the vector mode decays rapidly. On the other hand, the tensor mode can be observed as the polarization of CMB or the gravitational waves. The amplitude at the horizon crossing time is obtained as

$$\Delta^2_t\big|_{k=aH} = \frac{2}{\pi^2}\frac{H^2}{M_{\mathrm{P}}^2}\bigg|_{k=aH}. \tag{13}$$

Then the tensor-to-scalar ratio r of the power spectra is defined:

$$r := \frac{\Delta^2_t}{\Delta^2_{\mathcal{R}}}\bigg|_{k=aH} = 16\epsilon|_{k=aH}. \tag{14}$$

If the inflation is derived by the cosmological constant, the Hubble flow function $\epsilon = 0$ and the tensor-to-scalar ratio is also zero.

The observed values n_s and r are close to the case of the cosmological constant: $n_s = 0.968 \pm 0.006$ and $r \leq 0.09$ [6]. However, in that case the universe cannot stop their accelerated expansion and then any stars nor galaxies are not formed. From next section, we will review the slow-roll mechanism which avoid the problem of the cosmological constant model.

2.2 Single-field slow-roll model

Almost flat potential of a scalar field acts the role of "cosmological constant" depending on its height. The scalar field which induce the inflation is called inflaton. The action of the single-scalar slow-roll model is

$$S = \int \sqrt{-g}\,\mathrm{d}^4x \left(-\frac{M_{\mathrm{P}}^2}{2}R + \frac{1}{2}g^{\mu\nu}\partial_\mu\varphi\partial_\nu\varphi - V(\varphi)\right) \tag{15}$$

[5] Under the slow-roll approximation, the first Hubble flow function is equal to the potential slow-roll parameter ϵ_V, which we will see in Sec. 2.2.

where $M_{\rm P} := 1/\sqrt{8\pi G} \simeq 2.4 \times 10^{18}\,\mathrm{GeV}$ is the reduced Planck scale, φ is a scalar field[6] and $V(\varphi)$ is its potential. The equation of motion (EOM) becomes

$$\ddot{\varphi} + 3H\dot{\varphi} + V'(\varphi) = 0 \tag{16}$$

where the prime denotes the argument derivative.

If we set φ (or equivalently $V(\varphi)$) to a constant, we can easily reproduce the exponential expansion which is derived the cosmological constant. Therefore we take the following two conditions in the slow-roll approximation.

- The kinetic term is efficiently smaller than the potential height: $\dot{\varphi}^2 \ll V(\varphi)$.
- The acceleration term in EOM can be neglected: $|\ddot{\varphi}| \ll |3H\dot{\varphi}|, |V'(\varphi)\,|$.

Usually these conditions are expressed by potential slow-roll parameters:

$$\epsilon_V := \frac{M_{\rm P}^2}{2}\left(\frac{V'}{V}\right)^2 \ll 1, \qquad \eta_V := M_{\rm P}^2\frac{V''}{V} \ll \mathcal{O}(1)\,. \tag{17}$$

When ϵ_V or η_V becomes $\mathcal{O}(1)$, the inflation ends.

Let us approximate the tentor-to-scalar ratio r in terms of the potential slow-roll parameters. We can obtain the energy-momentum tensor for the scalar field which form is Eq. (3) with

$$\rho = \frac{1}{2}\dot{\varphi}^2 + V(\varphi)\,, \qquad P = \frac{1}{2}\dot{\varphi}^2 - V(\varphi)\,. \tag{18}$$

Here we consider the slow-roll approximation so that the first terms Eqs. (18) are neglected: $\rho \sim V$ and $P \sim -V$. From the first equations of Eqs. (4) and (18),

$$\epsilon := -\frac{\dot{H}}{H^2} = -\frac{\dot{\varphi}\frac{\mathrm{d}H}{\mathrm{d}\varphi}}{H^2} \sim \frac{M_{\rm P}^2}{2}\left(\frac{V'}{V}\right)^2 = \epsilon_V, \tag{19}$$

here we use $\dot{\varphi} \sim -V'/3H$. The tensor-to-scalar ratio is given by Eq. (14) and we get

$$r \sim 16\epsilon_V. \tag{20}$$

In this thesis, we never analyze the time evolution of $a(t)$ and we always use the potential slow-roll parameter instead of the Hubble flow-function. We will use this result in Sec. 4.1.

[6] Here we do not restrict φ to Higgs.

2.3 Nonminimal coupling model

2.3.1 Conformal transformation

The slow-roll model needs a nearly-flat scalar potential. However, for example, Higgs field which is a sole elementary scalar field in the SM has quartic potential at high-energy scales, and it cannot satisfy the slow-roll conditions (17). The nonminimal-coupling Higgs inflation is an idea that makes the shape of potential to be flat by coupling terms between the Higgs field and the Ricci scalar [9, 10]. In this section, the mechanism is reviewed.

Let us consider an action for the single scalar field model,

$$S = \int \sqrt{-g}\,\mathrm{d}^4x \left(-\frac{M_{\mathrm{P}}^2}{2} F_R(\varphi)\, R + \frac{1}{2} F_\Phi(\varphi)\, g^{\mu\nu}\partial_\mu\varphi\partial_\nu\varphi - V(\varphi) \right) \tag{21}$$

where $F_R(\varphi)$ is the nonminimal couplings between the scalar and the gravity. Here we also introduce the nonminimal couplings for kinetic term $F_\Phi(\varphi)$ for preparation of discussion later.[7] We assume the Z_2 symmetry of the action for simplicity. We also require the nonminimal coupling terms become unity at the electroweak scale in order to the theory match the SM. Namely they are written in the form

$$F_R(\varphi) = 1 + \xi_R \frac{\varphi^2}{M^2} + \mathcal{O}\left(\frac{\varphi^4}{M^4}\right), \qquad F_\Phi(\varphi) = 1 + \xi_\Phi \frac{\varphi^2}{M^2} + \mathcal{O}\left(\frac{\varphi^4}{M^4}\right) \tag{22}$$

where M is a typical scale of ultraviolet theory which has mass dimension one, and ξ_X is the first coupling constant in the nonminimal-coupling function.[8]

In this system (21), we can always redefine the metric (or equivalently the scalar field) and the manipulation is called conformal transformation. To make the action to have a form of Einstein-Hilbert action with keeping the whole action is invariant, we define a new metric as

$$g^{\mathrm{E}}_{\mu\nu} := F_R(\varphi)\, g_{\mu\nu}. \tag{23}$$

The new frame is called the Einstein frame while the un-transformed frame is called the Jordan frame. Hereafter the superscript (or subscript) "E" denotes the Einstein frame. In the Einstein frame, the action becomes

$$S = \int \sqrt{-g_{\mathrm{E}}}\,\mathrm{d}^4x \left[-\frac{M_{\mathrm{P}}^2}{2} R_{\mathrm{E}} + \frac{1}{2}\mathcal{G}^2(\varphi)\, g^{\mu\nu}_{\mathrm{E}}\partial_\mu\varphi\partial_\mu\varphi - \frac{V(\varphi)}{F_R(\varphi)^2} \right] \tag{24}$$

[7] In this case the pressure becomes $P(\varphi) = \frac{1}{2}F_\Phi(\varphi)\, g^{\mu\nu}\partial_\mu\varphi\partial_\nu\varphi - V(\varphi)$ and the energy density is $\rho(\varphi) = \frac{1}{2}F_\Phi(\varphi)\, g^{\mu\nu}\partial_\mu\varphi\partial_\nu\varphi + V(\varphi)$. For more generic action we can apply the similarly argument, see e.g. the author's previous work [49].

[8] The nonminimal coupling ξ between Higgs and Ricci scalar in the ordinary notation relates to ξ_R as $\xi = \xi_R M_{\mathrm{P}}^2/M^2$ [10].

where

$$\mathcal{G}(\varphi) := \sqrt{\frac{F_\Phi(\varphi)}{F_R(\varphi)} + \frac{3}{2}\left(\frac{M_\mathrm{P} F_R'(\varphi)}{F_R(\varphi)}\right)^2}. \tag{25}$$

We define the Einstein-frame potential in Eq. (24) as

$$U(\varphi) := \frac{V(\varphi)}{F_R(\varphi)^2} \tag{26}$$

for convenience.

Let a term $\propto \varphi^n$ be the most contributory term of the scalar potential $V(\varphi)$. If the most contributory term of $F_R(\varphi)$ is proportional to $\varphi^{n/2}$, the last term of Eq. (24) closes to a constant as φ becomes large [50]. Then nearly flat potential in the Einstein frame leads to the slow-roll inflation. Note that at the electroweak scale the nonminimal couplings (22) is sufficiently approximated to 1 thus F_R or F_Φ does not affect the physics today. Actually the field φ is not canonically normalized in the Einstein frame, and the change of EOM must be taken into account at high-energy scales; see next section for the details.

2.3.2 Classical dynamics in terms of Jordan-frame field

We consider the effect of the non-canonical coefficient of kinetic term (25) at the classical level. We assume that the classical metric in the Einstein frame is the Friedmann-Lemaître-Robertson-Walker metric:

$$g^\mathrm{E}_{\mu\nu}\mathrm{d}x^\mu \mathrm{d}x^\nu = -\mathrm{d}{t_\mathrm{E}}^2 + a_\mathrm{E}^2(t_\mathrm{E})\,\mathrm{d}\mathbf{x}^2. \tag{27}$$

The Hubble parameter in the Einstein frame is defined as

$$H_\mathrm{E} := \frac{1}{a_\mathrm{E}}\frac{\mathrm{d}a_\mathrm{E}}{\mathrm{d}t_\mathrm{E}} \tag{28}$$

and the universe expands with the rate H_E. It is also convenient to define the canonically normalized scalar field χ as

$$\mathrm{d}\chi = \mathcal{G}(\varphi)\,\mathrm{d}\varphi. \tag{29}$$

In this case the Einstein equations become the ordinary Friedmann equation:[9]

$$H_\mathrm{E}^2 = \frac{\rho_\mathrm{E}}{3M_\mathrm{P}^2}, \qquad \frac{\mathrm{d}\rho_\mathrm{E}}{\mathrm{d}t_\mathrm{E}} = -3\left(\rho_\mathrm{E} + p_\mathrm{E}\right)H_\mathrm{E}, \tag{30}$$

[9]The second equation is derived by the combine the Friedmann equations which have the form of Eq. (4).

where

$$\rho_{\rm E} = \frac{1}{2}\left(\frac{{\rm d}\chi}{{\rm d}t_{\rm E}}\right)^2 + U_{\rm E}(\varphi)\,, \qquad\qquad p_{\rm E} = \frac{1}{2}\left(\frac{{\rm d}\chi}{{\rm d}t_{\rm E}}\right)^2 - U_{\rm E}(\varphi)\,. \tag{31}$$

The Higgs-field equation becomes

$$\frac{{\rm d}^2\chi}{{\rm d}t_{\rm E}^2} + 3H_{\rm E}\frac{{\rm d}\chi}{{\rm d}t_{\rm E}} = -\frac{{\rm d}U_{\rm E}}{{\rm d}\chi} \tag{32}$$

and this is rewritten in terms of the Jordan-frame field as

$$\frac{{\rm d}^2\varphi}{{\rm d}t_{\rm E}^2} + \frac{{\rm d}\varphi}{{\rm d}t_{\rm E}}\left(3H_{\rm E} + \frac{\rm d}{{\rm d}t_{\rm E}}\ln\mathcal{G}\right) = -\frac{1}{\mathcal{G}^2}\frac{{\rm d}U_{\rm E}}{{\rm d}\varphi}. \tag{33}$$

We see the Jordan-frame field φ has an extra friction term $\frac{\rm d}{{\rm d}t_{\rm E}}\ln\mathcal{G}$ compared with the nonminimal-coupling case. This friction term changes the rolling speed of the field, but is the same order as the slow-roll parameter under the slow-roll condition, as we will see below.

Under the slow-roll condition, the Friedmann and Higgs-field equations become

$$3M_{\rm P}^2H_{\rm E}^2 = U_{\rm E}, \tag{34}$$

$$3H_{\rm E}\frac{{\rm d}\chi}{{\rm d}t_{\rm E}} = -\frac{{\rm d}U_{\rm E}}{{\rm d}\chi}. \tag{35}$$

We define the potential slow-roll parameters in the Einstein frame and write the slow-roll condition in terms of them,

$$\epsilon_V^{\rm E} := \frac{M_{\rm P}^2}{2U_{\rm E}^2}\left(\frac{{\rm d}U_{\rm E}}{{\rm d}\chi}\right)^2 = \frac{M_{\rm P}^2}{2U_{\rm E}^2\mathcal{G}^2}\left(\frac{{\rm d}U_{\rm E}}{{\rm d}\varphi}\right)^2 \ll 1, \tag{36}$$

$$\eta_V^{\rm E} := \frac{M_{\rm P}^2}{U_{\rm E}}\frac{{\rm d}^2U_{\rm E}}{{\rm d}\chi^2} = \frac{M_{\rm P}^2}{U_{\rm E}\mathcal{G}}\frac{\rm d}{{\rm d}\varphi}\left(\frac{1}{\mathcal{G}}\frac{{\rm d}U_{\rm E}}{{\rm d}\varphi}\right) \ll 1. \tag{37}$$

In terms of the Jordan-frame field, Eq. (35) becomes

$$3H_{\rm E}\frac{{\rm d}\varphi}{{\rm d}t_{\rm E}} = -\frac{1}{\mathcal{G}^2}\frac{{\rm d}U_{\rm E}}{{\rm d}\varphi}. \tag{38}$$

We define the effectual potential which takes into account the effect from $\mathcal{G}$ as

$$\mathcal{U}_{\rm E} := \int {\rm d}\varphi\frac{1}{\mathcal{G}^2}\frac{{\rm d}U_{\rm E}}{{\rm d}\varphi} + {\rm const.} \tag{39}$$

Then Eq. (38) is written as

$$3H_{\rm E}\frac{{\rm d}\varphi}{{\rm d}t_{\rm E}} = -\frac{{\rm d}\mathcal{U}_{\rm E}}{{\rm d}\varphi} \tag{40}$$

Using the potential (39), the slow-roll parameters can be rewritten as

$$\epsilon_V^{\mathrm{E}} = \frac{\mathcal{G}^2 M_{\mathrm{P}}^2}{2U_{\mathrm{E}}^2}\left(\frac{\mathrm{d}\mathcal{U}_{\mathrm{E}}}{\mathrm{d}\varphi}\right)^2, \tag{41}$$

$$\eta_V^{\mathrm{E}} = \frac{M_{\mathrm{P}}^2}{U_{\mathrm{E}}}\left(\frac{\mathrm{d}^2\mathcal{U}_{\mathrm{E}}}{\mathrm{d}\varphi^2} + \frac{\mathrm{d}\mathcal{U}_{\mathrm{E}}}{\mathrm{d}\varphi}\frac{\mathrm{d}}{\mathrm{d}\varphi}\ln\mathcal{G}\right). \tag{42}$$

We see that the extra friction is the same order as the slow-roll parameter from Eq. (42). In this paper, we omit the subscript E from U_{E} and $\mathcal{U}_{\mathrm{E}}$ which are always given in the Einstein frame.

3 Frame (in)dependence of the theory

We can flatten the quartic potential by the conformal transformation as introduced in Sec. 2.3. However, there appear problems when we consider the quantum loop corrections: we do not fully understand the renormalization under the existence of nonminimal couplings. In this section, we see the meaning of the field dependence of the renormalization scale. The content in this section is published in Ref. [51].

3.1 Frames at classical level

For our purpose, we will calculate fermion loop correction to the effective action in a simplified Higgs-Yukawa model.[10] We consider only the Higgs field φ and the fermion field ψ for simplicity. We also assumed that the action is invariant under a chiral Z_2 symmetry

$$\varphi \to -\varphi, \qquad \psi \to \gamma_5 \psi. \tag{43}$$

Then the action in Jordan frame becomes

$$S = \int \mathrm{d}^4x\sqrt{-g}\bigg[-\frac{M_{\rm P}^2}{2}F_R(\varphi)\,R + \frac{1}{2}F_\Phi(\varphi)\,g^{\mu\nu}\,\partial_\mu\varphi\,\partial_\nu\varphi - V(\varphi) \\ - F_\Psi(\varphi)\,\overline{\psi}\gamma^\mu D_\mu\psi - F_{\rm Y}(\varphi)\,y\varphi\overline{\psi}\psi\bigg], \tag{44}$$

where y is the Yukawa coupling[11] and $D_\mu = \partial_\mu + \Omega_\mu$ is the general covariant derivative on spinor, with Ω_μ being the spin-connection. The potential contains all the higher dimensional terms in general:

$$V(\varphi) = \sum_{n:\ \text{even},\ n\geq 0} \lambda_n \frac{\varphi^n}{M^{n-4}}. \tag{45}$$

Let us neglect the Higgs mass term because it is much smaller than the quartic coupling term at the large field values we consider. When we assume that all the higher order terms are small at $\varphi \sim M$, the potential becomes quartic at large φ and $V \ll M^4 \lesssim M_{\rm P}^4$: This is the case of the original Higgs inflation [10] which assumes that the potential (45) can be approximated by $V(\varphi) = \lambda_4\varphi^4$, namely $\lambda_n \ll 1$ for $n \neq 4$, at around the scale $\varphi \sim M \lesssim M_{\rm P}$.

[10] Actually, gauge-boson loop correction also affects the running of the Higgs self-coupling. However, the φ-dependent effective mass of the canonically normalized gauge boson has the same dependence in the Einstein frame as the effective mass of fermion; see e.g. Ref. [24]. Therefore the arguments for frame independence and for prescription dependence can be applied without modification after we include gauge-boson loops.

[11] This is related to the SM top Yukawa coupling y_t by $y = y_t/\sqrt{2}$

We also assume that all the nonminimal couplings $F_X(\varphi)$ approach to one when we take a weak-field limit $\varphi \to 0$:

$$F_X(\varphi) := 1 + \xi_X \frac{\varphi^2}{M^2} + \mathcal{O}\left(\frac{\varphi^4}{M^4}\right) \tag{46}$$

for $X = R$, Φ, Ψ and Y.

We obtain the Einstein-frame action by the field redefinition Eq. (23),

$$S = \int \mathrm{d}^4x\sqrt{-g_{\mathrm{E}}}\Bigg[- \frac{M_{\mathrm{P}}^2}{2}\mathcal{R}_{\mathrm{E}} + \frac{1}{2}\mathcal{G}^2(\varphi)\, g_{\mathrm{E}}^{\mu\nu}\, \partial_\mu\varphi\, \partial_\nu\varphi - \frac{V(\varphi)}{\left(F_R(\varphi)\right)^2} \\ - \frac{F_\Psi(\varphi)}{\left(F_R(\varphi)\right)^{3/2}}\overline{\psi}\gamma_{\mathrm{E}}^\mu D_\mu^{\mathrm{E}}\psi - \frac{F_{\mathrm{Y}}(\varphi)}{\left(F_R(\varphi)\right)^2} y\varphi\overline{\psi}\psi\Bigg]. \tag{47}$$

Hereafter in Sec. 3, the quantities without superscript or subscript "E" are given in the Jordan frame unless otherwise stated. We also use superscript or subscript "J" on quantities in the Jordan frames when it is preferable. Using the assumptions above, $U = V/F_R^2$ becomes constant in the large φ limit:

$$U \to \frac{\lambda_4}{\xi^2} M_{\mathrm{P}}^4 \tag{48}$$

where we used the relation in the footnote 8.

3.2 Effect of nonminimal coupling in quantum theory

Next we consider the quantum corrections to λ_n. In quantum theory, we need renormalization to cancel the divergences in the theory. The most contributory loop correction is the one from top quark. Thus we consider top-quark field as ψ hereafter, namely, we consider only one kind of fermion field and its loop correction. However, the following arguments does not depend on the number of fermion fields.

We write the bare Higgs potential as

$$V_{\mathrm{B}} := \sum_n \lambda_{n\mathrm{B}} \frac{\varphi^n}{M^{n-4}} \tag{49}$$

where $\lambda_{n\mathrm{B}}$ is the bare couplings. The full effective potential V is composed by the bare potential and the loop-correction to the potential ΔV_{eff}:

$$V := V_{\mathrm{B}} + \Delta V_{\mathrm{eff}}. \tag{50}$$

The divergences in V_{B} and in ΔV_{eff} must be canceled by each other so that the full potential is finite.

In the counterterm formalism, the renormalized Higgs potential V is computed as a sum of finite functions depending on the renormalization scale μ:

$$V = V_{\rm R}(\mu) + \Delta V_{\rm R}(\mu) \tag{51}$$

where $V_{\rm R}$ is the μ-dependent tree-level potential

$$V_{\rm R}(\varphi, \mu) := \sum_n \lambda_{n{\rm R}}(\mu)\, \frac{\varphi^n}{M^{n-4}} \tag{52}$$

and $\Delta V_{\rm R}$ is the loop correction. The running of $\lambda_{n{\rm R}}(\mu)$ is determined by the μ-independence of $V_{\rm B}$ after we determine the counterterm. Note that V is also independent of μ and we can choose μ arbitrarily.

In the SM, the choice $\mu \sim \varphi$ minimizes $\Delta V_{\rm R}$, then V can be approximated by the tree-level potential: $V \simeq V_{\rm R}|_{\mu=\varphi}$. However, in the nonminimal model, the corrections from the nonminimal couplings appears in general. For example, we may consider the nonminimal coupling term $\xi\varphi^2 R/M_{\rm P}^2$. Under the existence of this term, it has been said that there are two different "prescriptions" to approximate the renormalized Higgs potential to the tree-level one [20, 21, 22]

$$\mu \sim \begin{cases} \dfrac{\varphi}{\sqrt{1+\xi\frac{\varphi^2}{M_{\rm P}^2}}} & \text{(prescription I)}, \\ \varphi & \text{(prescription II)}. \end{cases} \tag{53}$$

We will review how to derive these expressions later.

A prescription is claimed to correspond to a φ-independent ultraviolet cutoff in a specific frame [20, 21], as mentioned in Introduction. The prescription II is has the same φ-dependence as the SM. On the other hand, it is said that the prescription I is preferred from the point of view of exact quantum scale invariance [52, 53, 54]. However, we cannot determine which prescription is suitable for our universe at present.

The different choice of prescription predicts the different value of observable such as the spectral index n_s [20]. It also results in the different size of the minimal coupling ξ to realize the inflation. For example, if we consider the criticality of the SM, the suitable values of Higgs self-coupling becomes $\mathcal{O}(10)$ for the prescription I and $\mathcal{O}(100)$ for the prescription II [23, 24]. It is rather curious because the entire Higgs potential V should not depend on μ, and then we consider that the current understanding of the prescriptions is not enough.

From the next section, we revisit the relation between the ultraviolet cutoff and the renormalization scale, and clarify that the different choice of the cutoff does not directly relate to the difference prescriptions.

3.3 Frame independence of effective action up to quartic divergence

In this subsection we show that the effective action is frame-independent up to quartic divergence if we properly take into account the change of the path integral measure as well as that of the ultraviolet cutoff, using the assumptions in the Section 3.1 for simplicity.

We evaluate only the one-loop correction from the fermion loop and ignore those from the graviton and φ loops. We also neglect all the corrections to other couplings y, ξ_X, etc., and hence do not distinguish the bare and renormalized couplings for them.

The metric redefinition (23) relates the short-distance cutoff lengths ℓ in Jordan and Einstein frames by

$$\ell_{\rm J}^2 = g_{\mu\nu}^{\rm J}\,\Delta x^\mu\,\Delta x^\nu = \frac{g_{\mu\nu}^{\rm E}}{F_R(\varphi)}\Delta x^\mu\,\Delta x^\nu = \frac{\ell_{\rm E}^2}{F_R(\varphi)} \tag{54}$$

where Δ denotes the difference. Namely, the ultraviolet cutoff scales $\Lambda_{\rm J/E}$ are related by

$$\Lambda_{\rm E}^2 = \frac{\Lambda_{\rm J}^2}{F_R(\varphi)}. \tag{55}$$

and we can choose either $\Lambda_{\rm J}$ or $\Lambda_{\rm E}$ to be independent of φ, but not both [20].

The frame independence of the effective potential has been verified in various ways.[12] Here we revisit and confirm it. The one-loop effective action induced by the fermion loop in the Jordan frame is given by

$$e^{i\Delta S_{\rm eff}^{\rm J}} := \int \mathcal{D}_{g_{\rm J}}\psi\;\mathcal{D}_{g_{\rm J}}\overline{\psi}\;\exp\left[i\int {\rm d}^4x\sqrt{-g_{\rm J}}\,\overline{\psi}\left(-F_\Psi \not{D}_{g_{\rm J}} - F_{\rm Y} y\varphi\right)\psi\right]. \tag{56}$$

Similarly, the one-loop effective action in the Einstein frame is

$$e^{i\Delta S_{\rm eff}^{\rm E}} := \int \mathcal{D}_{g_{\rm E}}\psi\;\mathcal{D}_{g_{\rm E}}\overline{\psi}\;\exp\left[i\int {\rm d}^4x\sqrt{-g_{\rm E}}\,\overline{\psi}\left(-\frac{F_\Psi}{F_R^{3/2}} \not{D}_{g_{\rm E}} - \frac{F_{\rm Y}}{F_R^2} y\varphi\right)\psi\right]. \tag{57}$$

The path integral measure $\mathcal{D}\psi$ has no unique definition. Here we use simply the distance in the functional space:

$$\|\delta\psi\|_{g_{\rm J}}^2 = \int {\rm d}^4x\sqrt{-g_{\rm J}}\,\delta\overline{\psi}\,\delta\psi \qquad \text{for } \mathcal{D}_{g_{\rm J}}\psi, \tag{58}$$

$$\|\delta\psi\|_{g_{\rm E}}^2 = \int {\rm d}^4x\sqrt{-g_{\rm E}}\,\delta\overline{\psi}\,\delta\psi \qquad \text{for } \mathcal{D}_{g_{\rm E}}\psi. \tag{59}$$

[12] For example, in Refs. [13, 18], the authors have obtained one-loop renormalization group equations for the tree-level action in both the Jordan and Einstein frames, and have found they agree; see also appendix of Ref. [17]. In Ref. [14], the authors verified that both the tree-level actions are equivalent when written in terms of dimensionless variables. In Ref. [15], it is shown that the one-loop divergent part of the effective potential in both frames coincide at on-shell. In Refs. [12, 16, 19], the authors have discussed frame independence of physical observables.

From Eqs. (23) and (58), we have

$$\|\delta\psi\|^2_{g_{\rm J}} = \int {\rm d}^4x\sqrt{-g_{\rm E}}\, F_R^{-2}\, \delta\overline{\psi}\, \delta\psi. \tag{60}$$

Then the functional measure satisfies

$$\begin{aligned}\mathcal{D}_{g_{\rm J}}\psi\ \mathcal{D}_{g_{\rm J}}\overline{\psi} &= \mathcal{D}_{g_{\rm E}}\psi\ \mathcal{D}_{g_{\rm E}}\overline{\psi}\ \left(\prod_x F_R^{-2}\right)^{-4} \\ &= \mathcal{D}_{g_{\rm E}}\psi\ \mathcal{D}_{g_{\rm E}}\overline{\psi}\ \exp\left[-4\ \mathop{\rm Tr}_{g_{\rm E},\Lambda_{\rm E}} \ln F_R^{-2}\right],\end{aligned} \tag{61}$$

where $\mathrm{Tr}_{g_{\rm E},\Lambda_{\rm E}}$ denotes the functional trace depending on the metric $g_{\rm E}$ and the cutoff $\Lambda_{\rm E}$, and the extra minus sign of -4 is from the Jacobian for fermionic variables. We can see that the functional measure $\mathcal{D}_{g_{\rm J}}\psi\ \mathcal{D}_{g_{\rm J}}\overline{\psi}$ produces the extra contribution factor

$$\exp\left[-4\ \mathop{\rm Tr}_{g_{\rm E},\Lambda_{\rm E}} \ln F_R^{-2}\right] \tag{62}$$

when we rewrite it in terms of Einstein-frame one. If we take the assumption that φ and $g_{\mu\nu}$ are slowly varying backgrounds so that they can be treated as constants in the computation of the effective action, it becomes

$$\begin{aligned}\exp\left[-4\ \mathop{\rm Tr}_{g_{\rm E},\Lambda_{\rm E}} \ln F_R^{-2}\right] &= \exp\left[-4i\int {\rm d}^4x\sqrt{-g_{\rm E}}\,\langle x\,|\,\ln F_R^{-2}\,|\,x\rangle_{\Lambda_{\rm E}}\right] \\ &= \exp\left[i\int {\rm d}^4x\sqrt{-g_{\rm E}}\left(-\frac{\Lambda_{\rm E}^4}{8\pi^2}\ln F_R^{-2}\right)\right]\end{aligned} \tag{63}$$

where we have used[13]

$$\langle x\,|\,x\rangle_{\Lambda_{\rm E}} = \int^{\Lambda_{\rm E}} \frac{{\rm d}^4p}{(2\pi)^4} = \int_0^{\Lambda_{\rm E}} \frac{2\pi^2p^3{\rm d}p}{(2\pi)^4} = \frac{\Lambda_{\rm E}^4}{32\pi^2}. \tag{64}$$

To see the frame independence of the effective action, let us rewrite the action (56) into the path integral in Einstein frame. It becomes

$$\begin{aligned}e^{i\Delta S^{\rm J}_{\rm eff}} &= \exp\left[-4\ \mathop{\rm Tr}_{g_{\rm E},\Lambda_{\rm E}} \ln F_R^{-2}\right] \\ &\quad\times \int \mathcal{D}_{g_{\rm E}}\psi\ \mathcal{D}_{g_{\rm E}}\overline{\psi}\ \exp\left[i\int {\rm d}^4x\sqrt{-g_{\rm E}}\,\overline{\psi}\left(-\frac{F_\Psi}{F_R^{3/2}}\not{D}_{g_{\rm E}} - \frac{F_{\rm Y}}{F_R^2}y\varphi\right)\psi\right] \\ &= \exp\left[-4\ \mathop{\rm Tr}_{g_{\rm E},\Lambda_{\rm E}} \ln F_R^{-2}\right] e^{i\Delta S^{\rm E}_{\rm eff}},\end{aligned} \tag{65}$$

[13]Here and hereafter, the momentum integral is taken in the Euclidean space.

and thus the effective action is frame-independent up to quartic divergence. This quartic divergence is absorbed into the renormalized couplings including the coefficients of higher dimensional terms. Before we see it, we verify the equality (65) through more explicit computations under the assumption that φ and $g_{\mu\nu}$ are slowly varying backgrounds. The effective action induced by fermion loop (56) becomes

$$\begin{aligned} e^{i\Delta S^{\rm J}_{\rm eff}} &= \operatorname*{Det}_{g_{\rm J},\Lambda_{\rm J}} \left(\frac{-F_\Psi \not{D}_{g_{\rm J}} - F_{\rm Y} y\varphi}{\mu_0} \right) \\ &= \exp\left[\operatorname*{Tr}_{g_{\rm J},\Lambda_{\rm J}} \ln\left(\frac{-F_\Psi \not{D}_{g_{\rm J}} - F_{\rm Y} y\varphi}{\mu_0} \right) \right] \\ &= \exp\left[4i \int {\rm d}^4x \sqrt{-g_{\rm J}} \int^{\Lambda_{\rm J}} \frac{{\rm d}^4p}{(2\pi)^4} \frac{1}{2} \ln\left(\frac{F_\Psi^2 p^2 + F_{\rm Y}^2 (y\varphi)^2}{\mu_0^2} \right) \right], \end{aligned} \tag{66}$$

where μ_0 is an arbitrary reference scale. We define the correction to the Jordan-frame potential[14]

$$\Delta V^{\rm J}_{\rm eff} := -4 \int^{\Lambda_{\rm J}} \frac{{\rm d}^4p}{(2\pi)^4} \frac{1}{2} \ln\left(\frac{F_\Psi^2 p^2 + F_{\rm Y}^2 (y\varphi)^2}{\mu_0^2} \right) \tag{67}$$

and it is computed as

$$\Delta V^{\rm J}_{\rm eff} = -\frac{1}{16\pi^2} \left\{ \Lambda_{\rm J}^4 \left[\ln\left(F_\Psi^2 \frac{\Lambda_{\rm J}^2 + \mathcal{M}_{\rm J}^2}{\mu_0^2} \right) - \frac{1}{2} \right] + \Lambda_{\rm J}^2 \mathcal{M}_{\rm J}^2 + \mathcal{M}_{\rm J}^4 \ln\left(\frac{\mathcal{M}_{\rm J}^2}{\Lambda_{\rm J}^2 + \mathcal{M}_{\rm J}^2} \right) \right\}, \tag{68}$$

where

$$\mathcal{M}_{\rm J}(\varphi) := y\varphi \frac{F_{\rm Y}(\varphi)}{F_\Psi(\varphi)} \tag{69}$$

is the field-dependent mass for canonically normalized fermion in the Jordan frame.

On the other hand, we may rewrite formally the effective action (66) with the Einstein-frame metric:

$$\begin{aligned} e^{i\Delta S^{\rm J}_{\rm eff}} &= \exp\left[i \int {\rm d}^4x \sqrt{-g_{\rm J}} \left(-\Delta V^{\rm J}_{\rm eff} \right) \right] \\ &= \exp\left[i \int {\rm d}^4x \sqrt{-g_{\rm E}} \left(-\frac{\Delta V^{\rm J}_{\rm eff}}{F_R^2} \right) \right] =: \exp\left[i \int {\rm d}^4x \sqrt{-g_{\rm E}} \left(-\Delta U^{\rm J}_{\rm eff} \right) \right] \end{aligned} \tag{70}$$

where we have defined the correction to the potential (26). The explicit form of $\Delta U^{\rm J}_{\rm eff}$ is

$$\begin{aligned} \Delta U^{\rm J}_{\rm eff} &:= \frac{\Delta V^{\rm J}_{\rm eff}}{F_R^2} \\ &= -\frac{1}{16\pi^2 F_R^2} \left\{ \Lambda_{\rm J}^4 \left[\ln\left(F_\Psi^2 \frac{\Lambda_{\rm J}^2 + \mathcal{M}_{\rm J}^2}{\mu_0^2} \right) - \frac{1}{2} \right] + \Lambda_{\rm J}^2 \mathcal{M}_{\rm J}^2 + \mathcal{M}_{\rm J}^4 \ln\left(\frac{\mathcal{M}_{\rm J}^2}{\Lambda_{\rm J}^2 + \mathcal{M}_{\rm J}^2} \right) \right\}. \end{aligned} \tag{71}$$

[14]For more realistic top quark loop, $\Delta V_{\rm eff}$ is multiplied by the color degrees of freedom $N_c = 3$.

Eq. (71) is the result of the transformed effective potential from Jordan frame to Einstein frame.

Next we consider the field redefinition (23) from the Einstein frame to Jordan frame. The Einstein-frame effective action induced by the fermion loop (57) becomes

$$\begin{aligned} e^{i\Delta S^{\rm E}_{\rm eff}} &= \exp\left[\operatorname*{Tr}_{g_{\rm E},\Lambda_{\rm E}} \ln\left(\frac{-\frac{F_\Psi}{F_R^{3/2}}\not{D}_{g_{\rm E}} - \frac{F_{\rm Y}}{F_R^2}y\varphi}{\mu_0}\right)\right] \\ &= \exp\left[4i\int {\rm d}^4x\sqrt{-g_{\rm E}}\int^{\Lambda_{\rm E}}\frac{{\rm d}^4p}{(2\pi)^4}\frac{1}{2}\ln\left(\frac{\frac{F_\Psi^2}{F_R^3}p^2+\frac{F_{\rm Y}^2}{F_R^4}(y\varphi)^2}{\mu_0^2}\right)\right]. \end{aligned} \tag{72}$$

We define the fermion loop correction to the potential (26) obtained with the measure $\mathcal{D}_{g_{\rm E}}\psi$ in the same way as Eq. (67):

$$\begin{aligned} \Delta U^{\rm E}_{\rm eff} &:= -4\int_0^{\Lambda_{\rm E}}\frac{{\rm d}^4p}{(2\pi)^4}\frac{1}{2}\ln\left(\frac{\frac{F_\Psi^2}{F_R^3}p^2+\frac{F_{\rm Y}^2}{F_R^4}y^2\varphi^2}{\mu_0^2}\right) \\ &= -\frac{1}{16\pi^2}\left\{\Lambda_{\rm E}^4\left[\ln\left(\frac{F_\Psi^2}{F_R^3}\frac{\Lambda_{\rm E}^2+\frac{\mathcal{M}_{\rm J}^2}{F_R}}{\mu_0^2}\right)-\frac{1}{2}\right]+\Lambda_{\rm E}^2\frac{\mathcal{M}_{\rm J}^2}{F_R}+\frac{\mathcal{M}_{\rm J}^4}{F_R^2}\ln\left(\frac{\frac{\mathcal{M}_{\rm J}^2}{F_R}}{\Lambda_{\rm E}^2+\frac{\mathcal{M}_{\rm J}^2}{F_R}}\right)\right\}. \end{aligned} \tag{73}$$

We can rewrite it in terms of the cutoff in Jordan frame by using the relation between the ultraviolet cutoff scales (55),

$$\Delta U^{\rm E}_{\rm eff} = -\frac{1}{16\pi^2F_R^2}\left\{\Lambda_{\rm J}^4\left[\ln\left(\frac{F_\Psi^2}{F_R^4}\frac{\Lambda_{\rm J}^2+\mathcal{M}_{\rm J}^2}{\mu_0^2}\right)-\frac{1}{2}\right]+\Lambda_{\rm J}^2\mathcal{M}_{\rm J}^2+\mathcal{M}_{\rm J}^4\ln\left(\frac{\mathcal{M}_{\rm J}^2}{\Lambda_{\rm J}^2+\mathcal{M}_{\rm J}^2}\right)\right\}. \tag{74}$$

Comparing the results (71) and (74), we obtain that

$$\Delta U^{\rm E}_{\rm eff} = \Delta U^{\rm J}_{\rm eff} - \frac{1}{16\pi^2}\Lambda_{\rm E}^4\ln F_R^{-4}. \tag{75}$$

We see that Eq. (75) is equivalent to Eq. (65) by using Eq. (63) and each definition of the effective potential. Note that the difference in (75) is quartically divergent, which will be subtracted by the renormalization.[15] In particular, this difference does not change the running of couplings, as we will see in Sec. 3.4.

[15] Here we use the result of the extra factor derived from a theory defined with a measure induced from the distance in the Jordan frame (58). The same argument can be applied when we start from a different theory defined with another measure induced from the distance (59). Then the Jordan-frame effective action will receive extra contribution from the change of measure, $\exp\left[4\operatorname*{Tr}_{g_{\rm J},\Lambda_{\rm J}}\ln F_R^{-2}\right]$, which again is quartic divergence and will make the difference only in the renormalization conditions.

We summarize the results in this subsection. Once we fix the path integral measure, $\mathcal{D}_{g_{\rm J}}\psi$ or $\mathcal{D}_{g_{\rm E}}\psi$, we obtain the same effective potential, $\Delta U^{\rm J}_{\rm eff}$ or $\Delta U^{\rm E}_{\rm eff}$, no matter in which frame we compute it: When we compute it in the Jordan frame, we obtain

$$\begin{aligned} e^{i\Delta S^{\rm J}_{\rm eff}} &= \exp\left[i\int {\rm d}^4x\sqrt{-g_{\rm J}}\left(-\Delta V^{\rm J}_{\rm eff}\right)\right] \\ &= \exp\left[i\int {\rm d}^4x\sqrt{-g_{\rm E}}\left(-\Delta U^{\rm J}_{\rm eff}\right)\right], \end{aligned} \tag{76}$$

while when we compute it in the Einstein frame,

$$\begin{aligned} e^{i\Delta S^{\rm J}_{\rm eff}} &= \exp\left[i\int {\rm d}^4x\sqrt{-g_{\rm E}}\left(-\frac{\Lambda_{\rm E}^4}{8\pi^2}\ln F_R^{-2}\right)\right] && \text{(The extra factor (63))} \\ &\quad\times \exp\left[i\int {\rm d}^4x\sqrt{-g_{\rm E}}\left(-\left(\Delta U^{\rm J}_{\rm eff}-\frac{\Lambda_{\rm E}^4}{16\pi^2}\ln F_R^{-4}\right)\right)\right] && \text{(The difference (74))} \\ &= \exp\left[i\int {\rm d}^4x\sqrt{-g_{\rm E}}\left(-\Delta U^{\rm J}_{\rm eff}\right)\right]. \end{aligned} \tag{77}$$

The effective action changes if we take another path integral measure. However, the difference is quartic divergence and we will see that it can be absorbed by the renormalization condition.

3.4 Prescriptions in the ordinary context

In the prescription I (II) in the original sense [20], we set $\Lambda_{\rm E}$ ($\Lambda_{\rm J}$) to be a φ-independent constant. First, in this subsection, we review how the prescription I or II in Eq. (53) appears in the ordinary context. Second, we show that the difference between two frames can be regarded as the difference of renormalization condition.

We consider the cutoff theory containing infinite number of higher dimensional terms. The effective potential should be a function of φ/M in the large cutoff limit $\Lambda_{\rm J}, \Lambda_{\rm E}\to\infty$ and the infinite number of bare couplings should be tuned so that the theory is renormalizable. We work in the counterterm formalism so that $\mathcal{M}_{\rm J}$ and F_Ψ are treated as finite renormalized quantities. We consider the theory defined by the path integral measure $\mathcal{D}_{g_{\rm J}}\psi$. This choice of theory is a just example: The same argument can be applied even when we consider the theory defined by the measure $\mathcal{D}_{g_{\rm E}}\psi$.

3.4.1 Prescription II in ordinary context

We start the prescription II for the convenience of explanation. The effective potential induced by the fermion loop (68) contains the quartic, quadratic, and logarithmic diver-

gences:

$$\Delta V_{\text{eff}} = -\frac{1}{16\pi^2}\left\{\Lambda_{\text{J}}^4\left[\ln\left(F_\Psi^2\frac{\Lambda_{\text{J}}^2}{\mu_0^2}\right)-\frac{1}{2}\right]+2\Lambda_{\text{J}}^2\mathcal{M}_{\text{J}}^2+\mathcal{M}_{\text{J}}^4\left(\ln\frac{\mathcal{M}_{\text{J}}^2}{\Lambda_{\text{J}}^2}-\frac{1}{2}\right)\right\} + \mathcal{O}\big(\Lambda_{\text{J}}^{-2}\big)\,. \tag{78}$$

The quartic and quadratic divergences in Eq. (78) can be simply subtracted by the counter term

$$V_{\text{power}}^{\text{c.t.}} = \frac{1}{16\pi^2}\left\{\Lambda_{\text{J}}^4\left[\ln\left(F_\Psi^2\frac{\Lambda_{\text{J}}^2}{\mu_0^2}\right)-\frac{1}{2}\right]+2\Lambda_{\text{J}}^2\mathcal{M}_{\text{J}}^2\right\}. \tag{79}$$

On the other hand, the counter term for the logarithmic divergence in Eq. (78) should be analytic around $\varphi = 0$ because we employ the analytic tree-level potential. Because $\ln\mathcal{M}_{\text{J}} = \ln\varphi + \cdots$ breaks the analyticity around $\varphi = 0$, a natural choice of the counter term that is analytic around $\varphi = 0$ would become

$$V_{\log}^{\text{c.t.II}} = \frac{\mathcal{M}_{\text{J}}^4}{16\pi^2}\ln\frac{\mu^2}{\Lambda_{\text{J}}^2}, \tag{80}$$

where μ is the renormalization scale. The resultant bare potential is obtained as

$$\begin{aligned} V_{\text{B}}^{\text{II}} &= V_{\text{R}}^{\text{II}} + V_{\text{power}}^{\text{c.t.}} + V_{\log}^{\text{c.t.II}} \\ &= V_{\text{R}}^{\text{II}} + \frac{1}{16\pi^2}\left\{\Lambda_{\text{J}}^4\left[\ln\left(F_\Psi^2\frac{\Lambda_{\text{J}}^2}{\mu_0^2}\right)-\frac{1}{2}\right]+2\Lambda_{\text{J}}^2\mathcal{M}_{\text{J}}^2+\mathcal{M}_{\text{J}}^4\ln\frac{\mu^2}{\Lambda_{\text{J}}^2}\right\}, \end{aligned} \tag{81}$$

where V_{R}^{II} is the μ-dependent tree-level potential in the counterterm formalism,

$$V_{\text{R}}^{\text{II}}(\varphi,\mu) := \sum_n \lambda_{n\text{R}}^{\text{II}}(\mu)\,\frac{\varphi^n}{M^{n-4}}. \tag{82}$$

The running of $\lambda_{n\text{R}}(\mu)$ is determined by the μ-independence of V_{B} via Eq. (81). Note that we can obtain the ordinary running of the quartic coupling

$$\frac{\mathrm{d}\lambda_{4\text{R}}(\mu)}{\mathrm{d}\ln\mu} = -\frac{y^4}{8\pi^2} \tag{83}$$

because $\mathcal{M}_{\text{J}} = y\varphi + \mathcal{O}\big(\varphi^3\big)$.

Then we obtain the full effective potential

$$\begin{aligned} V(\varphi) &= V_{\text{B}}^{\text{II}} + \Delta V_{\text{eff}} \\ &= V_{\text{R}}^{\text{II}}(\varphi,\mu) + \Delta V_{\text{R}}^{\text{II}}(\varphi,\mu)\,, \end{aligned} \tag{84}$$

where

$$\Delta V_{\rm R}^{\rm II}(\varphi,\mu) := -\frac{\left[\mathcal{M}_{\rm J}(\varphi)\right]^4}{16\pi^2}\left(\ln\frac{\left[\mathcal{M}_{\rm J}(\varphi)\right]^2}{\mu^2}-\frac{1}{2}\right) \tag{85}$$

is the one-loop correction in the counterterm formalism in the prescription II, and now both $V_{\rm R}^{\rm II}$ and $\Delta V_{\rm R}^{\rm II}$ are finite. To minimize the correction (85), we choose the renormalization scale[16]

$$\mu \sim \mathcal{M}_{\rm J}. \tag{86}$$

This result reproduces the prescription II in the sense of Eq. (53), $\mu\sim\varphi$, for $F_\Psi = F_{\rm Y} = 1$.

3.4.2 Prescription I in ordinary context

We can rewrite Eq. (78) by using Eq. (55):

$$\begin{aligned}\Delta V_{\rm eff} = &-\frac{F_R^2}{16\pi^2}\left\{\Lambda_{\rm E}^4\left[\ln\left(F_\Psi^2\frac{F_R\Lambda_{\rm E}^2}{\mu_0^2}\right)-\frac{1}{2}\right]+2\Lambda_{\rm E}^2\frac{\mathcal{M}_{\rm J}^2}{F_R}+\frac{\mathcal{M}_{\rm J}^4}{F_R^2}\left(\ln\frac{\mathcal{M}_{\rm J}^2/F_R}{\Lambda_{\rm E}^2}-\frac{1}{2}\right)\right\}\\ &+\mathcal{O}\left(\Lambda_{\rm E}^{-2}\right).\end{aligned} \tag{87}$$

The quartic and quadratic divergences are canceled by the same counter term (79), but it is more natural to cancel the logarithmic divergence by

$$V_{\log}^{\rm c.t.I} = \frac{\mathcal{M}_{\rm J}^4}{16\pi^2}\ln\frac{\mu^2}{\Lambda_{\rm E}^2} \tag{88}$$

instead of Eq. (80). Then the bare potential becomes

$$\begin{aligned}V_{\rm B}^{\rm I} &= V_{\rm R}^{\rm I} + V_{\rm power}^{\rm c.t.} + V_{\log}^{\rm c.t.I}\\ &= V_{\rm R}^{\rm I} + \frac{1}{16\pi^2}\left\{\Lambda_{\rm E}^4F_R^2\left[\ln\left(F_\Psi^2\frac{F_R\Lambda_{\rm E}^2}{\mu_0^2}\right)-\frac{1}{2}\right]+2\Lambda_{\rm E}^2F_R\mathcal{M}_{\rm J}^2+\mathcal{M}_{\rm J}^4\ln\frac{\mu^2}{\Lambda_{\rm E}^2}\right\},\end{aligned} \tag{89}$$

and we obtain

$$\begin{aligned}V(\varphi) &= V_{\rm B}^{\rm I} + \Delta V_{\rm eff}\\ &= V_{\rm R}^{\rm I}(\varphi,\mu) + \Delta V_{\rm R}^{\rm I}(\varphi,\mu),\end{aligned} \tag{90}$$

where

$$\Delta V_{\rm R}^{\rm I}(\varphi,\mu) := -\frac{\left[\mathcal{M}_{\rm J}(\varphi)\right]^4}{16\pi^2}\left(\ln\frac{\left[\mathcal{M}_{\rm J}(\varphi)\right]^2/F_R}{\mu^2}-\frac{1}{2}\right). \tag{91}$$

[16]The constant $-1/2$ is scheme-dependent and does not affect our argument here.

The running of quartic coupling is fixed by the μ-independence of V and becomes the same as in Eq. (83): The φ^4 term is not affected by $\ln F_R$ because $F_R = 1 + \mathcal{O}(\varphi^2)$.

To minimize Eq. (91), the renormalization scale is chosen as

$$\mu \sim \frac{\mathcal{M}_{\rm J}}{\sqrt{F_R}}. \tag{92}$$

This result reproduces the prescription I in the sense of Eq. (53) for $F_\Psi = F_{\rm Y} = 1$.

To summarize, we have started from the measure (58), and computed the one-loop correction (68) in each frame. We have derived the renormalization scales that reproduce both prescriptions from the same effective potential which is defined in the Jordan frame. Actually the change of path measure (61) introduces a trace anomaly in addition to Eq. (63), but it is taken into account as a form of the logarithmic ultraviolet cutoff dependence in Eq. (68).

3.5 The difference of the prescriptions

In this subsection, we clarify how the difference of the prescriptions in Eq. (53) arises in the ordinary context. And then we will show that the difference can be absorbed into the choice from infinitely many possibilities of the coefficients of higher dimensional terms in the tree-level potential. We also use the counterterm formalism in this subsection and assume the each finite term in potential are analytic around $\varphi = 0$.

To come to the point, the difference between prescriptions I and II comes from that of the subtractions of logarithmic divergence in Eqs. (80) and (88):

$$V_{\rm log}^{\rm c.t.I} - V_{\rm log}^{\rm c.t.II} = \frac{\mathcal{M}_{\rm J}^4}{16\pi^2} \ln \frac{\Lambda_{\rm J}^2}{\Lambda_{\rm E}^2}. \tag{93}$$

Using Eq. (55), it becomes

$$V_{\rm log}^{\rm c.t.I} - V_{\rm log}^{\rm c.t.II} = \frac{\mathcal{M}_{\rm J}^4}{16\pi^2} \ln F_R = \frac{\xi_R y^4}{16\pi^2} \frac{\varphi^6}{M^2} + \cdots . \tag{94}$$

Note that the difference (94) is analytic around $\varphi = 0$ and that it has only higher order terms with $n \geq 6$. This difference corresponds to the finite renormalization of $V_{\rm R}$, as we will see below.

Let us determine the form of renormalized potential. The renormalized potential $V_{\rm R}$ in Eq. (84) or (90),

$$V_{\rm R}(\varphi, \mu) = \sum_{n:\ \text{even},\ n \geq 0} \lambda_{n{\rm R}}(\mu) \frac{\varphi^n}{M^{n-4}}, \tag{95}$$

can take arbitrary form in theory. To reproduce the ordinary Higgs inflation [10], the infinite number of bare couplings are tuned so that all the couplings $\lambda_{n\mathrm{R}}(\mu)$ with $n \neq 4$ are suppressed at $\mu \sim M$ as mentioned:

$$V_{\mathrm{R}}(\varphi, \mu)|_{\mu \sim M} \simeq \lambda_{4\mathrm{R}}(\mu)\, \varphi^4. \tag{96}$$

Substituting Eq. (96) into Eqs. (84) and (90), we obtain the Higgs potential in the prescriptions II and I in the ordinary context, respectively:

$$V^{\mathrm{II}} = \lambda_{4\mathrm{R}}(\mu)\, \varphi^4 - \frac{\mathcal{M}_{\mathrm{J}}^4}{16\pi^2} \left(\ln \frac{\mathcal{M}_{\mathrm{J}}^2}{\mu^2} - \frac{1}{2} \right), \tag{97}$$

$$V^{\mathrm{I}} = \lambda_{4\mathrm{R}}(\mu)\, \varphi^4 - \frac{\mathcal{M}_{\mathrm{J}}^4}{16\pi^2} \left(\ln \frac{\mathcal{M}_{\mathrm{J}}^2/F_R}{\mu^2} - \frac{1}{2} \right). \tag{98}$$

Actually, we can obtain the potential of the form of V^{I} in Eq. (98) even when we employ the counter term $V_{\log}^{\mathrm{c.t.II}}$ in Eq. (80). This is the case if we choose the following form of the tree-level potential V_{R} in Eq. (84),

$$V_{\mathrm{R}}(\varphi, \mu) = \lambda_{4\mathrm{R}}(\mu)\, \varphi^4 + \frac{\left[\mathcal{M}_{\mathrm{J}}(\varphi)\right]^4}{16\pi^2} \ln F_R(\varphi)\,, \tag{99}$$

instead of the form (96). Note that the second term in the right-hand side of Eq. (99) modifies only the higher dimensional terms of φ^n for $n \geq 6$. By assuming the proper tree-level potentials (96) or (99), we may obtain the forms (97) or (98) from the same counter term $V_{\log}^{\mathrm{c.t.II}}$ in Eq. (80).

There are infinitely many possibilities for the tree-level potential unless we fix the underlying ultraviolet-finite theory. Therefore there is no necessity to suppose one of the two tree-level potential as the proper one if we consider only the low-energy effective field theory.

In conclusion, for a given renormalized tree-level action, the difference of the prescriptions (53) can be understood as that of the logarithmic counter terms (94). In other words, the different counter terms (80) and (88) lead to the different scales (86) and (92) that minimize the radiative corrections.

3.6 Required value of coupling for each prescription

Finally, we review the required coupling size by each case of the prescriptions. Let us consider more realistic running of the quartic coupling in the SM:

$$V_{\mathrm{SM}} = \lambda_{4\mathrm{R}}(\mu)\, \varphi^4 + \Delta V_{\mathrm{R}}(\varphi, \mu)\,, \tag{100}$$

where $\Delta V_{\rm R}$ is the finite correction (85) or (91) in the counterterm formalism. In the SM, the beta-function of Higgs self-coupling

$$\beta_{4\rm R} := \frac{\rm d}{{\rm d}\ln\mu}\lambda_{4\rm R} \tag{101}$$

changes its sign from negative to positive around the scale $\mu_{\rm min} \sim 10^{17}\,{\rm GeV}$ (the SM criticality). Therefore we may approximate the coupling as [23, 24]

$$\lambda_{4\rm R}(\mu) \approx \lambda_{4\rm R}^{\rm min} + b_{4\rm R}\left(\ln\frac{\mu}{\mu_{\rm min}}\right)^2, \tag{102}$$

where

$$b_{4\rm R} \simeq \frac{0.1}{\left(16\pi^2\right)^2} \simeq 5\times 10^{-6} \tag{103}$$

is computed within the SM. The negative $\beta_{4\rm R}$ for $\mu < \mu_{\rm min}$ is dominated by top-quark loop, while the positive $\beta_{4\rm R}$ for $\mu > \mu_{\rm min}$ by the ${\rm U}(1)_Y$ and ${\rm SU}(2)_L$ gauge-boson loops.

The contribution of top-quark loop comes from its mass $\mathcal{M}_{\rm J} = y\varphi F_{\rm Y}/F_\Psi = y\varphi$, where we assume $F_{\rm Y} = F_\Psi = 1$. In the prescription I in the sense of Eq. (53) (in other words, in Eq. (98) with the tree-level potential (96)), we get the constant μ in the large φ limit,

$$\mu \sim \frac{\mathcal{M}_{\rm J}}{\sqrt{F_R}} \to \frac{M_{\rm P}}{\sqrt{\xi}}, \tag{104}$$

and the effective quartic coupling $\lambda_{4\rm R}(\mu)|_{\mu\sim\mathcal{M}_{\rm J}/\sqrt{F_R}}$ stops running for large φ [22].[17] This mechanism makes the potential even flatter. Combining with the SM criticality, it can earn a sufficiently large e-folding number for smaller $\xi \sim 10$ [23, 43, 44, 24]. On the other hand, in the prescription II needs larger coupling $\xi \sim 10^2$ [23, 24] even under the SM criticality because $\lambda_{4\rm R}(\mu)|_{\mu\sim\mathcal{M}_{\rm J}}$ does not stop running.

3.7 Various Higgs-inflation models

As we have seen, it is artificial to limit the prescriptions to these two and there is no reason we must choose one at the moment. Moreover even if we take the simple form of the tree-level potential (96) in Eq. (84) or (90), we still have freedom to choose any form of $F_X(\varphi)$s. Actually, we have found that we may obtain the desirable potential even in prescription II in ordinary context when there are nonminimal couplings between φ and the gauge kinetic term. In this section, we show such inflation model and other possible inflation mechanisms using nonminimal couplings.

[17] If $F_{\rm Y} = 1 + \xi_{\rm Y}\varphi^2/M^2$ and $F_\Psi = 1 + \xi_\Psi\varphi^2/M^2$, we obtain

$$\mu \sim \frac{\mathcal{M}_{\rm J}}{\sqrt{F_R}} \to \frac{\xi_{\rm Y}}{\sqrt{\xi}\xi_\Psi} M_{\rm P}$$

instead of Eq. (104).

3.7.1 Flattened Higgs potential by kinetic function

In Sec. 3.6, we have shown the mechanism that the top-quark loop contribution leads to the flat potential. Here we show that the contribution from the gauge-boson loop can similarly make the flat potential.

Let us consider the Lagrangian of the simplified Higgs-gauge model:

$$\mathcal{L} = \frac{M_{\rm P}^2}{2} F_R(\varphi)\, R - \frac{1}{2}\left(F_\Phi g^{\mu\nu}\partial_\mu\varphi\partial_\nu\varphi + A_\mu A_\nu \varphi^2\right) - V(\varphi) - \frac{F_g(\varphi)}{4g^2} F_{\mu\nu}F^{\mu\nu} \tag{105}$$

where g is the gauge coupling and $F_{\rm g}$ is the coefficient function of φ in front of the gauge kinetic term. Then the contribution of the gauge-boson loop is through [24]

$$\mathcal{M}_{\rm J}^{\rm gauge} = g\varphi\sqrt{\frac{F_\Phi}{F_{\rm g}}}. \tag{106}$$

When we raise the scale beyond $\mu > \mu_{\rm min}$ in the SM, the top Yukawa coupling becomes smaller and smaller. To the first approximation, the running at $\mu > \mu_{\rm min}$ is governed by the gauge-boson loop. In the prescription II in the ordinary context (Eq. (97) with the tree-level potential (96)), the effective potential becomes

$$V_{\rm SM} = \lambda_{\rm 4R}(\mu)\,\varphi^4\big|_{\mu=\mathcal{M}_{\rm J}^{\rm gauge}}. \tag{107}$$

When we assume that $F_\Phi \simeq 1$, we obtain in the large-φ limit,

$$\mathcal{M}_{\rm J}^{\rm gauge} = \frac{g\varphi}{\sqrt{1+\xi_{\rm g}\frac{\varphi^2}{M^2}}} \to \frac{g}{\sqrt{\xi_{\rm g}}}M. \tag{108}$$

This can be used in the prescription II in the ordinary context as an alternative mechanism to Eq. (104) in order to stop the running of quartic coupling $\lambda_{\rm 4R}(\mu)|_{\mu\sim\mathcal{M}_{\rm J}^{\rm gauge}}$ for large φ. The φ-dependent mass (108) takes the same form as the prescription I in Eq. (53) and the analysis becomes almost identical to those in Ref. [24] if we set $\xi_{\rm g} = \xi_R$ and $M = M_{\rm P}$.

On the other hand, when the top Yukawa contribution is non-negligible in the action (44), one may further introduce e.g.

$$F_\Psi(\varphi) = \sqrt{1+2\xi_\Psi\frac{\varphi^2}{M^2}} = 1 + \xi_\Psi\frac{\varphi^2}{M^2} - \frac{\xi_\Psi^2}{2}\frac{\varphi^4}{M^4} + \frac{\xi_\Psi^3}{2}\frac{\varphi^6}{M^6} + \cdots \tag{109}$$

together with $F_{\rm Y} = 1$, which stops running due to the top contribution too:

$$\mathcal{M}_{\rm J} = \frac{y\varphi}{\sqrt{1+2\xi_\Psi\frac{\varphi^2}{M^2}}} \to \frac{y}{\sqrt{2\xi_\Psi}}M. \tag{110}$$

3.7.2 Ordinary Higgs inflation in prescription II

In Ref. [24], the authors have spelled out the result from prescriptions I and II in the ordinary context. In Sec. 3.6 we mentioned that the former prescription I allows smaller $\xi := \xi_R M_{\rm P}^2/M^2 \sim 10$ because the coupling stops running for $\varphi \gg M/\sqrt{\xi_R}$:

$$\mu \sim \frac{\varphi}{\sqrt{F_R}} \to \frac{M}{\sqrt{\xi_R}}. \tag{111}$$

On the other hand, though the prescription II needs $\xi \sim 10^2$, it can have a chaotic inflation since the effectual potential (39) becomes

$$\mathcal{U} \sim \text{const.} + \frac{\beta_\lambda M_{\rm P}^2}{48\xi^2}\varphi^2, \tag{112}$$

due to

$$\mathcal{G} \to \frac{\sqrt{6}M_{\rm P}}{\varphi} \tag{113}$$

for large ξ_R.

3.7.3 Chaotic-like inflation by large $\boldsymbol{\xi_\Phi}$

When we have large ξ_Φ only, in particular with $F_R = 1$, we may get

$$\mathcal{G} \to \sqrt{\xi_\Phi}\,\frac{\varphi}{M}. \tag{114}$$

We note in this case $U = V = \frac{\lambda}{4}\varphi^4$. Therefore the effectual potential (39) becomes

$$\mathcal{U} = \text{const.} + \frac{\lambda M^2}{2\xi_\Phi}\varphi^2. \tag{115}$$

This can cause a chaotic inflation when $\lambda/\xi_\Phi \ll 1$ [55].

4 Lower bound on tensor-to-scalar ratio

In this section, we consider a Higgs-inflation model that the inflation occurred at higher energy scale than the cutoff of low-energy effective theory and calculate the lower bound on the tensor-to-scalar ratio r. To obtain the lower bound on r, we do not need the details of the model except for the mechanism is the slow-rolling: the nonminimal Higgs inflation is also included in our consideration.

Dark matter is one of unsolved big problem in cosmology. In this thesis we do not investigate what it is, but take a Higgs-portal Z_2 scalar field as one of the simplest realizations. We calculate the lower bound on r and the upper bound on dark-matter mass for the model. Later we also introduce the heavy right-handed neutrinos via the seesaw mechanism [56, 57] and perform the same analysis. These analyses is also available in the author's work [58].

4.1 Inflation at higher scale than cutoff

In this subsection, we show how to obtain the lower bound on r, extending the analysis in Ref. [59].

For the slow-roll inflation, the effect of nonminimal coupling on the Higgs potential needs to be large. Let us consider $F_R(\varphi) = 1 + \xi\varphi^2/M_{\rm P}^2$ in Eq. (21) for example. The Einstein-frame potential (26) can be approximated to a constant at $\xi\varphi^2/M_{\rm P}^2 \gtrsim 1$. In other words, the low-energy effective theory such as the SM is valid only below the effective Planck scale $\sim M_{\rm P}/\sqrt{\xi}$.

Not limited in such case, a low-energy effective theory has some cutoff scale[18] Λ in general. In our analysis, we assume that at $\varphi < \Lambda$, there is a valid renormalizable low-energy effective field theory which we defined later. At $\varphi \geq \Lambda$, we assume that a field direction extrapolated from the low-energy Higgs field has led to slow-roll inflation there. We do not make any other assumptions on the theory at $\varphi \geq \Lambda$.

We do not predict precisely the cosmological parameters such as the spectral index n_s and the tensor-to-scalar ratio r in this case because the inflaton potential above Λ is not specified. However, we may still put a lower bound on r from the highest value of the Higgs potential in the region $\varphi < \Lambda$, as we will describe.

In the slow-roll inflation, the observable amplitude of the scalar perturbation A_s and r are written in terms of the potential slow-roll parameter ϵ_V and the potential height $V_{\rm inf}$ by using Eqs. (4) and (18):

$$A_s = \frac{1}{24\pi^2}\frac{1}{\epsilon_V}\frac{V_{\rm inf}}{M_{\rm P}^4}. \tag{116}$$

[18] Note that this "cutoff" scale Λ is conceptually different from the cutoffs in Sec. 3, which denotes the upper limit of the momentum integral.

This can be derived from Eqs. (4) and (11). Eliminating ϵ_V by using Eq. (20), we obtain the relation between r and $V_{\rm inf}$:

$$r = \frac{2}{3\pi^2}\frac{1}{A_s}\frac{V_{\rm inf}}{M_{\rm P}^4}. \tag{117}$$

This is a simple linear relation because the value of A_s is fixed by the CMB observation.

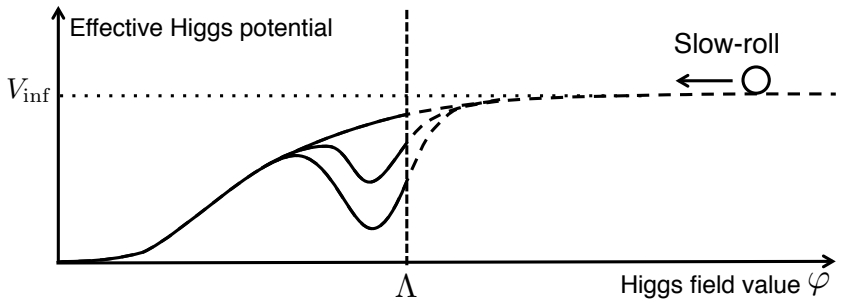

Figure 1: Schematic figure for the Higgs field as an inflaton

Now we consider the slow-roll inflation occurred by a field direction extrapolated from the low-energy Higgs field[19] above a scale Λ; see Fig. 1. Above Λ, the Higgs potential becomes flat by some mechanism such as nonminimal couplings, string theory, etc. After the end of inflation, the slow-roll condition on the Higgs field is violated and the field continues to roll on the potential down to the electroweak (EW) scale. In order not to prevent the rolling down to the EW scale, the maximum value of the effective potential in the region $\varphi \leq \Lambda$, which we define $V_{\varphi\leq\Lambda}^{\rm max}$, must be smaller than the potential height during the inflation $V_{\rm inf}$:

$$V_{\varphi\leq\Lambda}^{\rm max} < V_{\rm inf}. \tag{118}$$

From Eqs. (117) and (118),

$$r > r_{\rm bound} := \frac{2}{3\pi^2}\frac{1}{A_s}\frac{V_{\varphi\leq\Lambda}^{\rm max}}{M_{\rm P}^4}. \tag{119}$$

Thus, we obtain the lower bound on r from the value of $V_{\varphi\leq\Lambda}^{\rm max}$ only.[20] This can be evaluated from the renormalization group equations (RGEs) for the low-energy effective theory. Note that even if there exists a local maximum with its height smaller than $V_{\rm inf}$, it does not prevent the rolling down because the slow-roll condition is already violated.[21]

[19] Hereafter we call the field direction "Higgs field" for simplicity.

[20] We assume that the reheating temperature is lower than $V_{\varphi\leq\Lambda}^{\rm max}$. We also assume that the decay rate of Higgs boson to top quark (or vice versa) is sufficiently small.

[21] To be exact, we should consider additionally the thermal effect and the friction; see the discussion in Sec. 5.

Actually, this bound depends strongly on Λ. In our analysis we take $\Lambda = 10^{17}\,\mathrm{GeV}$ for the reasons below.

- The original nonminimal Higgs-inflation model requires a large nonminimal coupling $\xi \sim 10^4$ between the Higgs-squared[22] $\Phi^\dagger\Phi$ and the Ricci scalar R to realize the observed r and n_s [9, 10]. However, such large coupling requires a new physics above the scale $\sim M_\mathrm{P}/\xi$ for perturbative unitarity [60, 61, 62, 63]. It is also reported that the large nonminimal coupling in Higgs inflation might have problems: generation of the higher derivative terms [64] and violation of the preheating dynamics [65]. However, the nonminimal coupling can be reduced to $\mathcal{O}\big(10^2\big)$ if we consider the SM criticality [23, 24]. In this case, the energy scale where the inflation occurred becomes high. Then the effective Planck scale $\sim M_\mathrm{P}/\sqrt{\xi}$ becomes $\mathcal{O}\big(10^{17}\big)$ GeV.

- In our analysis, we do not make any assumptions on the high-energy theory except for the slow-roll inflation. Therefore we may consider other models instead of the nonminimal model. For example, it is reported that the string theory may lead to the inflation without the large nonminimal coupling [59, 66]. The typical string scale is $\mathcal{O}\big(10^{17}\big)$ GeV, and the low-energy effective theory is valid only below it.

If we want to know the lower bound on the tensor-to-scalar ratio for another cutoff scale, we just rescale the results we have calculated; see Sec. 4.4.2 for the details.

We cannot calculate the spectral index n_s because we do not specify the mechanism of inflation. However, if the inflation has occurred at $\varphi \geq \Lambda$, we can obtain the lower bound on r for any inflation model.

When all the other nonminimal couplings are not particularly large as well, $\xi_X < 10^2$, the renormalizable low-energy effective field theory is reliable up to $10^{17}\,\mathrm{GeV}$. Hereafter, we take $\Lambda = 10^{17}\,\mathrm{GeV}$.

4.2 Z_2 Higgs-portal scalar model

From this section, we will take a more concrete model, Higgs-portal Z_2 scalar model, for the numerical calculation of the bounds. In this model, the Z_2 scalar singlet S is considered as the dark matter. Below the scale Λ, the matter Lagrangian is

$$\mathcal{L}_\mathrm{matter} = \mathcal{L}_\mathrm{SM} + \frac{1}{2}(\partial_\mu S)^2 - \frac{1}{2}m_S^2 S^2 - \frac{\lambda_S}{4!}S^4 - \frac{\kappa}{2}S^2\Phi^\dagger\Phi. \tag{120}$$

Hereafter we use $\varphi = \sqrt{2\Phi^\dagger\Phi}$. The dark-matter mass is given by

$$m_\mathrm{DM}^2 = m_S^2 + \frac{\kappa v^2}{2}, \tag{121}$$

[22] In the terms of φ, $\varphi = \sqrt{2\Phi^\dagger\Phi}$.

where $v \simeq 246\,\mathrm{GeV}$ is the Higgs vacuum expectation value (VEV).

We assume that S does not acquire a Planck scale VEV and thus does not affect the inflation; the inflation is driven by the Higgs field, but we do not fix the details of potential shape. We also assume that m_S is small and neglect it. In our analysis we do not consider the possibility that m_{DM} is as lighter as the Higgs mass. In the non-resonant region, the relic density of the dark matter constrains κ as [67, 68]

$$\log_{10}\kappa \simeq -3.63 + 1.04\log_{10}\frac{m_{\mathrm{DM}}}{\mathrm{GeV}}. \tag{122}$$

In the region of our interest, $0.1 \lesssim \kappa \lesssim 0.5$, Eq. (122) becomes roughly $m_{\mathrm{DM}} \simeq \kappa \times 3.2\,\mathrm{TeV}$.

m_{DM} is constrained by the spin-independent cross section for the dark-matter–nucleon scattering [67, 68]:

$$\begin{aligned}\sigma_{\mathrm{SI}} &= \frac{\kappa^2 f_N^2}{4\pi}\left(\frac{m_n m_{\mathrm{DM}}}{m_n + m_{\mathrm{DM}}}\right)^2 \frac{m_n^2}{m_H^4 m_{\mathrm{DM}}^2} \\ &\simeq 6.5\times 10^{-46}\,(m_{\mathrm{DM}})^{0.08}\ \mathrm{cm}^2\end{aligned} \tag{123}$$

where $f_N = \frac{2}{9} + \frac{7}{9}\sum_{q=u,d,s} f_q \sim 0.345$ is the overall coupling, $m_n \sim 940\,\mathrm{MeV}$ is the nucleon mass, and $m_H = 125.09\,\mathrm{GeV}$ is the Higgs mass. We use Eq. (122) in the last step. The dependency on m_{DM} is small on comparison σ_{SI} with the observational data. The current constraints of dark-matter mass by the XENON1T experiment [69] for Eq. (123) are shown in Fig. 2. The constraints from other experiments are shown in Table. 1.

Experiment	Lower bound on m_{DM}	Corresponding value of κ
LUX [71]	$\sim 720\,\mathrm{GeV}$	~ 0.22
XENON1T [69]	$\sim 870\,\mathrm{GeV}$	~ 0.27
PandaX-II [70]	$\sim 1\,\mathrm{TeV}$	~ 0.31

Table 1: The lower bounds on dark-matter mass (90% C.L.).

We may employ the nonminimal coupling between Higgs and Ricci scalar to cause the inflation at the scale above Λ. In our analysis, its effect on the low-energy physics is ignored because we assume the nonminimal couplings are small: For example, a nonminimal coupling term $\xi\varphi^2/M_{\mathrm{P}}^2 \lesssim \mathcal{O}(1)$ for $\xi \lesssim \mathcal{O}\big(10^2\big)$ at $\varphi \le \Lambda \sim 10^{17}\,\mathrm{GeV}$.

4.3 Method of analysis

Thing to do to obtain the lower bound on r is to calculate the maximum value of the Higgs effective potential $V_{\varphi\le\Lambda}$. Then the parameters λ_S and κ affects the result through the renormalization group (RG) running of the Higgs quartic coupling, while m_S does not.

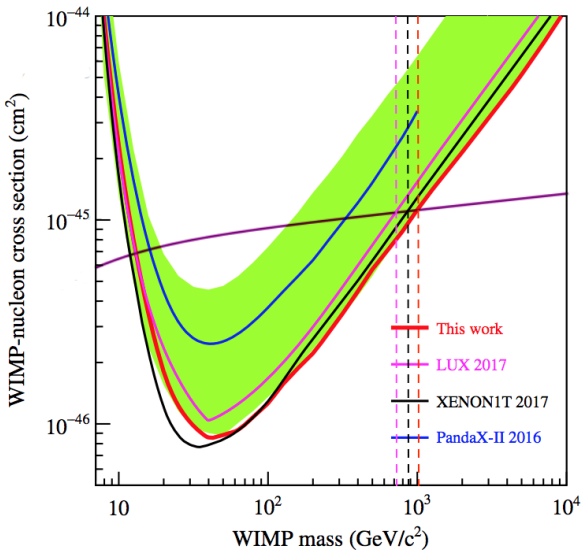

Figure 2: Fig. 5 (a) in Ref. [70]. The upper side of the curves is excluded for 90% C.L. We superpose the purple line which stands for Eq. (123). The dashed vertical lines are mere marks to see the mass constraint.

It is more practical that we estimate the top-quark mass from the observational relation between $m_{\rm DM}$ (equivalently κ) and the bound on r, than estimating $m_{\rm DM}$ by observing the top-quark mass and $r_{\rm bound}$. Although the top-quark mass has not been precisely determined, for the numerical calculation we need to employ the pole mass of the top quark m_t as an input parameter to solve the RGEs. The most precise knowledge about the top-quark mass is the Monte-Carlo mass $m_t^{\rm MC}$ which is obtained by Monte Carlo simulation of the whole process [72],

$$m_t^{\rm MC} = 173.1 \pm 0.6\,{\rm GeV}. \tag{124}$$

The pole mass of the top quark m_t which is the pole position of the propagator is also derived from the cross-section measurements [72]

$$m_t = 173.5 \pm 1.1\,{\rm GeV}. \tag{125}$$

We may not use simply the Monte-Carlo mass because it is not a parameter of theory, and the relation between $m_t^{\rm MC}$ and m_t is still unclear.[23] Hereafter we analyze in two conservative ranges including a central value of mass:

$$171\,{\rm GeV} \leq m_t \leq 176\,{\rm GeV}, \tag{126}$$

$$169\,{\rm GeV} \leq m_t \leq 178\,{\rm GeV}, \tag{127}$$

[23] There remains uncertainty at least of 1 GeV; see e.g. Ref. [73] for a recent review.

which roughly corresponds to 2σ and 4σ ranges, respectively.

In summary, the input parameters for RGEs are λ_S, κ, and the pole mass of top quark m_t. Here and hereafter the couplings are given at the scale $\mu = m_t$ unless otherwise stated. We analyze the two-loop RGEs and neglect the wave-function renormalization $\Gamma(\varphi)$ given in Eq. (146) for numerical computation. We determine $V_{\varphi\leq\Lambda}$ from the obtained running couplings. The largest possible deviation due to $\Gamma(\varphi)$ is also estimated by setting $\varphi = \Lambda$. The details of calculation are summarized in Appendix A.

To investigate the most conservative lower bound on r, we exclude the parameter region in which $V_{\varphi\leq\Lambda}$ becomes negative, namely the region that $V^{\rm min}_{\varphi\leq\Lambda} < 0$ in our results. This non-negative condition is the only condition to determine the lowest value of $V^{\rm max}_{\varphi\leq\Lambda}$. Practically, we take the false position method to exclude these regions.

The lower bound on r may slightly be affected when we relax the non-negative condition on the Higgs potential; e.g. taking into account the thermal correction or replacing it with the vacuum meta-stability. However, the bound comes from the maximum value of effective Higgs potential, rather than the minimum. Thus the lower bound on r would be reduced only by a factor of few even if we allow the negative value of the potential minimum of the order of the height of the potential maximum. Of course we should make sure that finally the electroweak vacuum is chosen in the late time in such a case.

We also exclude the parameter region in which the perturbativity of couplings is violated. For the perturbativity, we demand that all the couplings are smaller than $\sqrt{4\pi} \simeq 3.5$ in all the region $\varphi \leq \Lambda$. This condition corresponds to the requirement for κ to be $\kappa \lesssim 0.5$, equivalently

$$m_{\rm DM} \lesssim 1.6\,{\rm TeV}, \tag{128}$$

for $\lambda_S = 0$.[24] We shade in the region where perturbativity is violated in the result plots which will be shown. In this paper, we restrict to the case $\lambda_S = 0$ except for Fig. 3 (b) in which we instead take $\lambda_S = 0.6$ for comparison. We will see in Fig. 3 (b) that the large λ_S tends to narrower the allowed region. Therefore, it is more conservative to set $\lambda_S = 0$.

From next subsection, we will show plots of allowed regions in r-$m_{\rm DM}$ plane obtained by calculating $V^{\rm max}_{\varphi\leq\Lambda}$ as a function of κ for each fixed set of (λ_S, m_t) and converting κ to $m_{\rm DM}$ via Eq. (122).

4.4 Analysis without heavy right-handed neutrinos

4.4.1 Result plots

We plot the allowed region in r-$m_{\rm DM}$ plane for $\lambda_S = 0$ in Fig. 3 (a). The region above each line is only allowed. A solid and dashed lines denote the results without and with

[24] See Fig. 1 in Ref. [68] for the allowed region in the λ_S–κ plane. This upper bound on κ (or equivalently $m_{\rm DM}$) depends on the value λ_S, while its dependency on Λ is small; see Sec. 4.4.2.

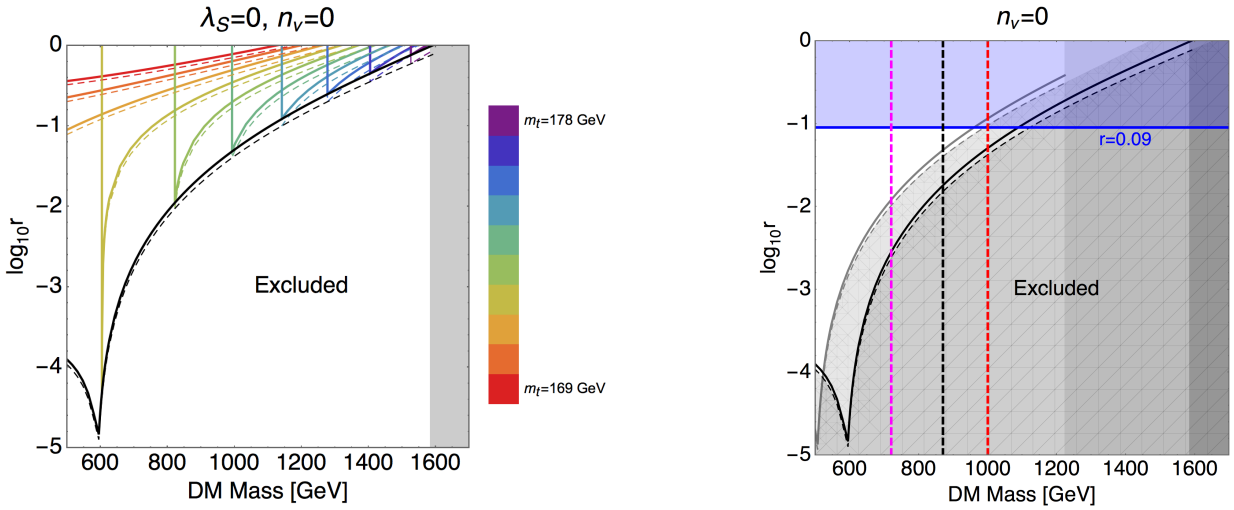

(a) (b)

Figure 3: (a) Allowed regions for $\lambda_S = 0$. The region above each rainbow-colored line is allowed for a given m_t. Each vertical line denotes the lower bound on $m_{\rm DM}$ from the positivity of potential: $V_{\varphi \leq \Lambda} > 0$. In the region $m_{\rm DM} \gtrsim 1.6\,{\rm TeV}$, the perturbativity is violated. See Fig. 11 for the corresponding plot with right-handed neutrinos.
(b) Excluded regions for $\lambda_S = 0$ (below black line) and $\lambda_S = 0.6$ (below gray line). The vertical black (gray) shade in $m_{\rm DM} \gtrsim 1.6\,{\rm GeV}$ ($m_{\rm DM} \gtrsim 1.2\,{\rm TeV}$) is excluded by the perturbativity for $\lambda_S = 0$ (0.6). The blue line denotes $r = 0.09$ and its the upper side is excluded [6]. The dashed vertical lines denote the lower bounds on dark matter mass, $m_{\rm DM} = 720\,{\rm GeV}$ from LUX [71] (magenta), $m_{\rm DM} = 870\,{\rm GeV}$ from XENON1T [69] (black) and $m_{\rm DM} = 1\,{\rm TeV}$ from PandaX-II [70] (red). The left-hand side of each dash line has been excluded.

the effects of Γ, respectively. The rainbow-colored lines correspond to each m_t value. The black line is the envelope of the rainbow-colored lines and gives the lower bound on r for each $m_{\rm DM}$ when one varies m_t. To understand the form of envelope, we need to know how the Higgs potential changes its shape with parameters, see Sec. 4.6. In Fig. 3 (b), We plot the excluded regions for all value of m_t when $\lambda_S = 0$ and $\lambda_S = 0.6$. The larger λ_S reduces the allowed range of r and κ, as mentioned.

From Fig. 3, the Planck constraint $r < 0.09$ [6] puts bounds on m_t and $m_{\rm DM}$:

$$171\,\mathrm{GeV} < m_t < 175\,\mathrm{GeV}, \tag{129}$$

$$m_{\rm DM} \lesssim 1.1\,\mathrm{TeV}, \tag{130}$$

for $\lambda_S = 0$. This bound on $m_{\rm DM}$ is stricter than the perturbativity bound (128). The lower bound on r is determined by the dark-matter mass constraint in Table. 1. If we take the lower bound from the LUX experiment [71], $m_{\rm DM} \gtrsim 720\,\mathrm{GeV}$, we obtain a lower bound: $r \gtrsim 0.0025$. For the lower bound on $m_{\rm DM}$ by the XENON1T experiment [69], $m_{\rm DM} \gtrsim 870\,\mathrm{GeV}$, $r \gtrsim 0.016$ is obtained. If we take the strictest bound by the PandaX-II experiment [70], $m_{\rm DM} \gtrsim 1\,\mathrm{TeV}$, we obtain the lower bound on tensor-to-scalar ratio

$$r \gtrsim 0.040 \tag{131}$$

and the bound on top-quark mass

$$174\,\mathrm{GeV} < m_t < 175\,\mathrm{GeV}. \tag{132}$$

If near-future experiments such as the POLARBEAR-2 [74], LiteBIRD [75] and CORE [76] find new constraints or concrete value of dark-matter mass, this lower-bound on r may be stricter, or the model breaks down because the allowed region of dark-matter mass disappears. This model also can be tested by the search of r directly. From Fig. 3 (b) we see that the cases of $\lambda_S = 0.6$ has been excluded.

4.4.2 Dependency on the cutoff scale

From the reasons listed in Sec. 4.1, we believe that the cutoff scale is $\Lambda \sim 10^{17}\,\mathrm{GeV}$ if it exists, and we have taken $\Lambda = 10^{17}\,\mathrm{GeV}$ in our analysis. However, we show an example result for another value of Λ because the analysis is sensitive to the cutoff Λ. Let us call a different cutoff scale Λ'. Naively, the maximum value of potential for the theory with Λ' is estimated as

$$V^{\max}_{\varphi \le \Lambda'} \sim \left(\frac{\Lambda'}{\Lambda}\right)^4 V^{\max}_{\varphi \le \Lambda} \tag{133}$$

because $V \propto \varphi^4$ at high-energy scales.

We show the result for the case of $\Lambda' = 5 \times 10^{16}\,\mathrm{GeV}$ in Fig. 4.

From Fig. 4, we find the following facts.

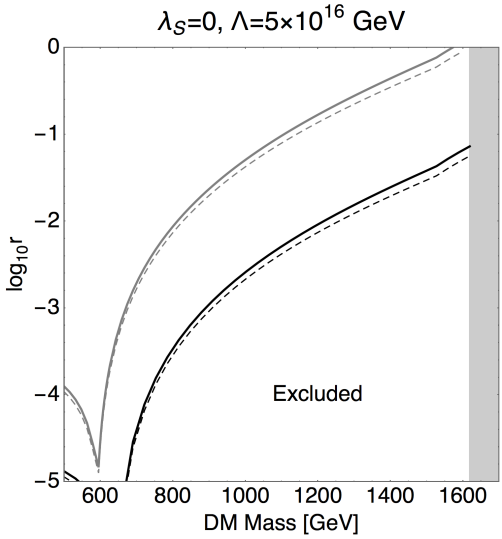

Figure 4: The lower bound on the tensor-to-scalar ratio for $\lambda_S = 0$, $\Lambda' = 5 \times 10^{16}\,\mathrm{GeV}$ (black) and $\lambda_S = 0$, $\Lambda = 10^{17}\,\mathrm{GeV}$ (gray). Here we restrict the top-quark mass range as the 4σ (Eq. (127)). The bend at $m_{\mathrm{DM}} \gtrsim 1.5\,\mathrm{TeV}$ is due to the upper limit $m_t = 178\,\mathrm{GeV}$.

- The tensor-to-scalar ratio r is roughly rescaled by (up to) $\left(\Lambda'/\Lambda\right)^4 = 1/16$ as we estimated.
- There exists the upper bound on m_{DM} around 1.6 TeV due to the Landau pole. Its dependence on the cutoff is small and the bound does not exceed to 1.7 TeV ($\kappa \sim 0.53$) even if the cutoff is $5 \times 10^{16}\,\mathrm{GeV}$.[25]
- m_{DM} where r takes its lowest value does not strongly changed when we change Λ.

In particular, it is significant that this model is excluded without any other assumptions if we observe $m_{\mathrm{DM}} > 1.7\,\mathrm{GeV}$.[26]

4.5 Analysis with right-handed neutrinos

4.5.1 Seesaw mechanism

In the SM, the neutrinos are massless particle. However, the neutrino oscillation has been experimentally discovered [77, 78] and now we consider that the neutrinos have mass.

[25]The usual Higgs inflation model leads to the effective cutoff scale $\Lambda \sim 10^{16}\,\mathrm{GeV}$. Even in that case the upper bound on m_{DM} does not move. This upper bound on m_{DM} hardly depends on even the right-handed neutrino mass, as we will see in Sec. 4.5.

[26]This upper limit of dark-matter mass is mainly fixed by the value that we decide as the Landau pole. We take the threshold as $\sqrt{4\pi}$ in order to guarantee the perturbativity. If we take smaller threshold, the upper bound on dark-matter mass becomes more severe.

As the mechanism to make the SM neutrinos have their masses, we adopt the seesaw mechanism [56, 57] and introduce the heavy right-handed neutrinos:

$$\mathcal{L}_{\rm RH} = \bar{\nu}_R i\gamma^\mu \partial_\mu \nu_R - \frac{1}{2} M_R \bar{\nu}_R^c \nu_R - \left(y_\nu \bar{L} \Phi^\dagger \nu_R + \text{h.c.} \right) \tag{134}$$

where we omit the indices of the generations. Because these right-handed neutrinos may modify the shape of effective Higgs potential, we analyze their loop corrections and calculate the lower bound on r.

After the spontaneous symmetry breaking, the Yukawa term in Eq. (134) acquire the Dirac mass $m_{\rm D} = y_\nu v/\sqrt{2}$. Then the mass term becomes

$$\frac{1}{2} \begin{pmatrix} \bar{\nu}_L & \bar{\nu}_R^c \end{pmatrix} \begin{pmatrix} 0 & m_{\rm D} \\ m_{\rm D}^T & M_R \end{pmatrix} \begin{pmatrix} \nu_L^c \\ \nu_R \end{pmatrix} + \text{h.c.} \tag{135}$$

and the neutrino-mass matrix $\tilde{m}_\nu$ turns to

$$\tilde{m}_\nu \simeq -m_{\rm D} \frac{1}{M_R} m_{\rm D}^T. \tag{136}$$

The observational constraints on the left-handed neutrino mass in the SM are following:

- The upper bound on the sum of masses. E.g. the 2σ upper bound from the TT-only analysis is $\sum_i m_i < 0.715\,\text{eV}$, while that from the TT+lensing+ext gives $\sum_i m_i < 0.234\,\text{eV}$ [6]. In this thesis, we assume roughly $\sum_i m_i \lesssim 0.3\,\text{eV}$.
- The mass-squared differences $m_2^2 - m_1^2 = (7.37^{+0.17}_{-0.16}) \times 10^{-5}\,\text{eV}^2$ and $m_3^2 - (m_2^2 + m_1^2)/2 = (2.525^{+0.042}_{-0.030}) \times 10^{-3}\,\text{eV}^2$ (both are 1σ C.L.) [79].

Here we used the notation of Ref. [79] for the mass eigenstates of left-handed neutrinos m_i. Using the constraints of the mass-squared differences, we find the three typical patterns of mass relations:

1. Normal Hierarchy (NH, m_1 the lightest),
2. Inverted Hierarchy (IH, m_3 the lightest),
3. Degenerate (all masses comparable),

where m_i $(i = 1, 2, 3)$ is the neutrino mass of mass eigenstate. In hierarchycal cases, the mass pattern is most hierarchical when the lightest one is 0. In Degenerate case, any neutrino mass do not go beyond $\sim 0.1\,\text{eV}$ from the upper bound on the sum of neutrino masses.

	m_1 [eV]	m_2 [eV]	m_3 [eV]	Pattern
1. Normal Hierarchy	0 (set)	8.6×10^{-3}	5.1×10^{-2}	$m_1 \ll m_2 < m_3$
2. Inverted Hierarchy	5.0×10^{-2}	5.0×10^{-2}	0 (set)	$m_1 \simeq m_2 \gg m_3$
3. Degenerate (NO)	0.1 (set)	1.0×10^{-1}	1.1×10^{-1}	$m_1 \simeq m_2 \simeq m_3$
3. Degenerate (IO)	1.1×10^{-1}	1.1×10^{-1}	0.1 (set)	$m_1 \simeq m_2 \simeq m_3$

Table 2: Neutrino masses obtained by using the absolute values of mass-squared differences in Ref. [79].

In Table 2, we show the mass pattern by setting the lightest one to be massless for the cases of Normal/Inverted Hierarchy, and to be 0.1 eV for Degenerate. For the three cases, we approximate the heaviest n_ν neutrinos as having a common mass m_ν and the remaining $3 - n_\nu$ ones as being massless as shown in Table 3.[27]

	Number of effective ν	Common mass m_ν [eV]
1. Normal Hierarchy	$n_\nu = 1$	5.1×10^{-2}
2. Inverted Hierarchy	$n_\nu = 2$	5.0×10^{-2}
3. Degenerate	$n_\nu = 3$	1.1×10^{-1}

Table 3: Common neutrino mass that we use as input.

The existence of heavy right-handed neutrino adds the right-handed neutrino mass $M_{\mathrm{R},i}$ ($i = 1, 2, 3$) to the input parameters of RGEs. We assume that $M_{\mathrm{R},i}$s are identical, $M_{\mathrm{R},i} = M_\mathrm{R}$, for simplicity. Then the Yukawa coupling of neutrino is given by the see-saw mechanism:

$$y_\nu = \sqrt{2 m_\nu M_\mathrm{R}}/v. \tag{137}$$

We show the β-functions in this case in Appendix A. Although we assume the mass of the heaviest left-handed neutrino as Table 3 in our analysis, there is no need to solve RGEs for other value of m_ν again. The reason is that m_ν and M_R have the one-to-one correspondence (137): If the observed constraint on m_ν changes, we can obtain the corresponding M_R constraint just rescaling the result.

[27] If we want to consider a different m_ν, we may simply rescale the right-handed neutrino mass M_R in our results, since $m_\nu \propto M_\mathrm{R}^{-1}$ by the seesaw mechanism.

Note that the right-handed neutrinos do not affect the dark-matter density because they decay to the Higgs boson and the left-handed neutrinos; we consider the dark matter consists of the Higgs-portal scalar S only. We also ignore the effect by the leptogenesis by the right-handed neutrinos.

4.5.2 Lower bound on r for each $M_{\rm R}$

Normal Hierarchy We show the results for Normal Hierarchy, $n_\nu = 1$, in Fig. 5. The right-handed neutrino mass $M_{\rm R}$ is fixed in each panel: 10^{13}, 10^{14}, $10^{14.4}\,(\simeq 2.5\times10^{14})$, $10^{14.5}\,(\simeq 3.2\times10^{14})$, $10^{14.6}\,(\simeq 4.0\times10^{14})$, and $10^{14.7}\,(\simeq 5.0\times10^{14})$ in units of GeV. The bold line in each panel is the envelope of the m_t-fixed rainbow-colored lines, and gives the lower bound on r for the fixed $M_{\rm R}$. Note that the thick line is obtained by tuning one parameter m_t for fixed $M_{\rm R}$, and its minimum corresponds to the two parameter tuning of m_t and $m_{\rm DM}$. The color of envelope in each panel corresponds to the color of Fig. 6, the plots for more general values of $M_{\rm R}$; we will explain the details later.

From Fig. 5, for a given lower bound on m_t, we see that the larger $M_{\rm R}$ is, the smaller the allowed range of $m_{\rm DM}$ becomes. This is because the right-handed neutrinos and the top quark have a similar effect on the Higgs potential: They drives the Higgs quartic coupling smaller through the RG running towards high scales, and therefore they tend to make the Higgs potential negative if they both are heavy. In this case, the vacuum stability is violated before the breakdown of perturbativity.

We also see that the value of $m_{\rm DM}$ at the minimum point of the envelope becomes larger as $M_{\rm R}$ becomes larger: For example, the minimum points are at $m_{\rm DM}\sim 600\,{\rm GeV}$ in the case of $M_{\rm R} = 10^{13}\,{\rm GeV}$, and $m_{\rm DM}\sim 870\,{\rm GeV}$ in the case of $M_{\rm R} = 10^{14}\,{\rm GeV}$, etc. In particular, it goes beyond the perturbativity bound when $M_{\rm R} = 10^{14.7}\,{\rm GeV}$. It indicates that we have a stringent lower bound, $r \gtrsim 10^{-2}$, with the heavy right-handed neutrino mass $M_{\rm R} \gtrsim 5\times10^{14}\,{\rm GeV}$. On the other hand, the result with $M_{\rm R} \lesssim 10^{13}\,{\rm GeV}$ is almost the same as the case without right-handed neutrinos shown in Fig. 3 (a).

In Fig. 6, we plot the theoretical lower bounds on r for various $M_{\rm R}$ when we allow the top-quark pole mass within $171\,{\rm GeV} < m_t < 176\,{\rm GeV}$ and $169\,{\rm GeV} < m_t < 178\,{\rm GeV}$. Each colored line corresponds to the envelope denoted by the thick colored line in Fig. 5. We also give the envelope of these lines, which gives the allowed region for varying m_t and $M_{\rm R}$.

Practically, it takes high computational cost to obtain the lower bound on r (denoted by the black line) for all parameter space. Therefore we have plotted the approximated envelope as follows:

1. Each $M_{\rm R}$-fixed line has a minimum. Make an interpolating function which linearly joins all these minimum points.

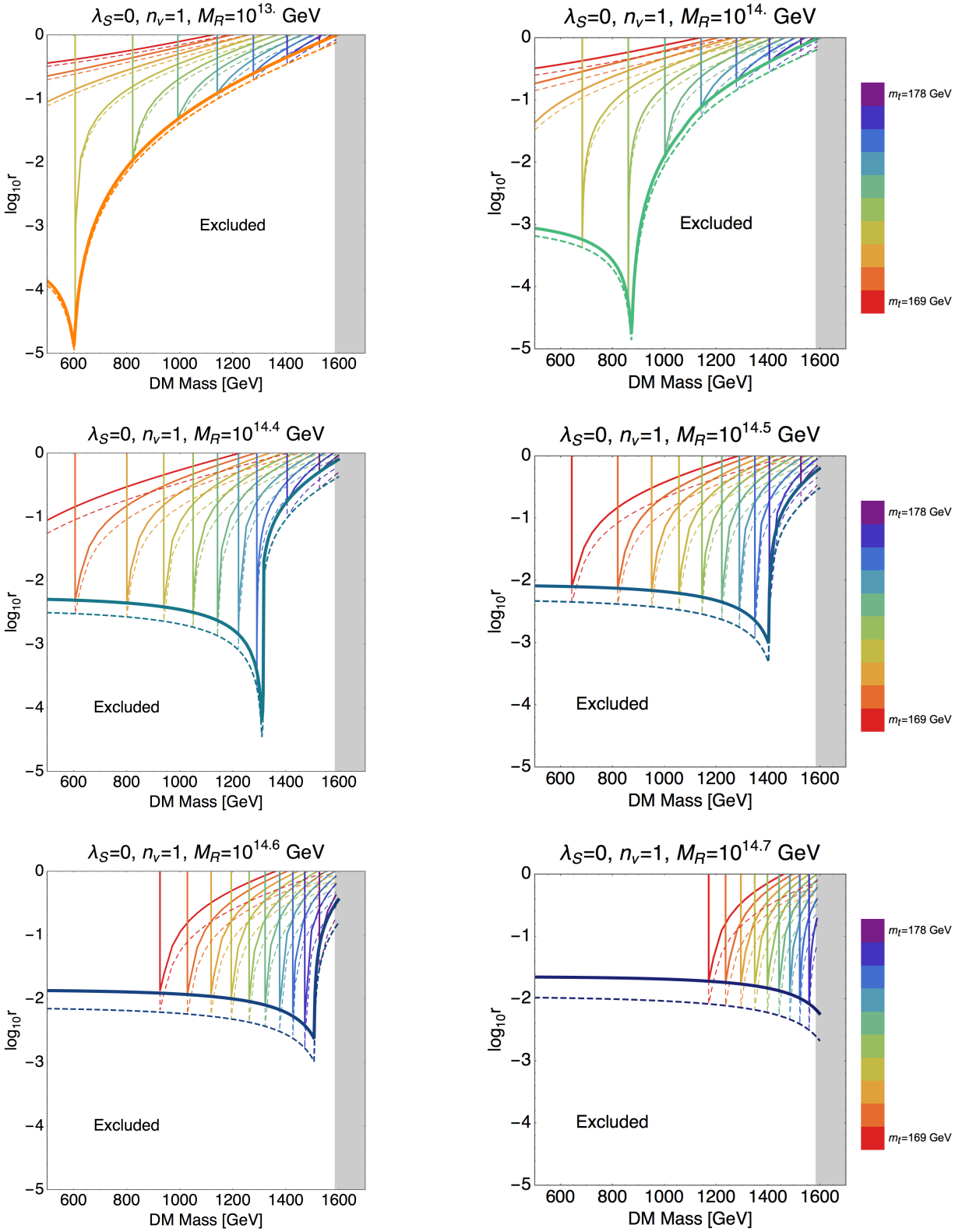

Figure 5: Allowed region for Normal Hierarchy with $\lambda_S = 0$.

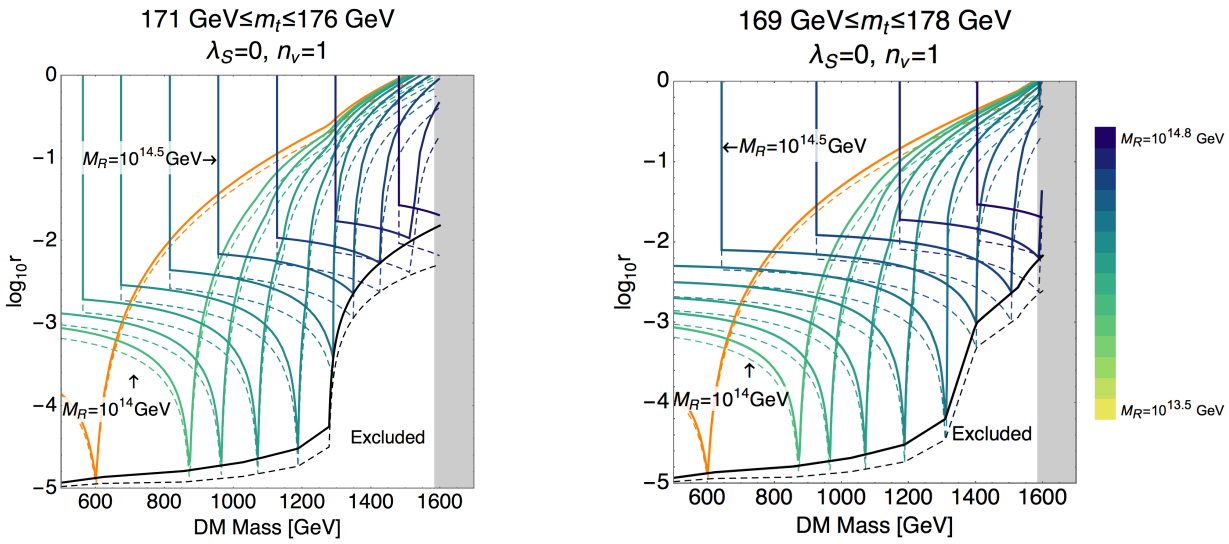

(a) (b)

Figure 6: The allowed region for Normal Hierarchy.
(a) The lower bound on r for each fixed $M_{\rm R}$ (colored) and their envelope (black) with $\lambda_S = 0$ and $171\,{\rm GeV} < m_t < 176\,{\rm GeV}$. The orange line is for $M_{\rm R} = 10^{13}$ GeV. The vertical colored line comes from the lower end, $m_t > 171\,{\rm GeV}$.
(b) The same plot for $\lambda_S = 0$ and $169\,{\rm GeV} < m_t < 178\,{\rm GeV}$.

2. Each m_t-fixed line[28] has a minimum. Make another interpolating function which linearly joins all these minimum points.

3. Make a function that chooses the smaller value of these two interpolating functions for each $m_{\rm DM}$.

4. In large $m_{\rm DM}$ region, we replace the interpolated bound with the lower bound determined by the maximal m_t.

We note that these interpolating functions may be wrong in the extrapolated regions $m_{\rm DM} < 600\,{\rm GeV}$ and $m_{\rm DM} > 1600\,{\rm GeV}$ because they evaluated only for $600\,{\rm GeV} < m_{\rm DM} < 1600\,{\rm GeV}$. However, this is insignificant because these regions are already excluded by the direct dark-matter search and by the perturbativity. We use this procedure hereafter to obtain black envelopes, but the last step is not taken in Sec. 4.5.3.

We explain the envelope denoted by the black line in Fig. 6 (a):

- The allowed region expand to

$$r \gtrsim 10^{-5} \tag{138}$$

  from the $n_\nu = 0$ case in Eq. (131). This is because the loop corrections of heavy right-handed neutrinos reduce $V^{\rm max}_{\varphi\le\Lambda}$.

- In the region near the envelope denoted by the black line, the two input parameters m_t and $M_{\rm R}$ are simultaneously tuned for a given $m_{\rm DM}$ to minimize the potential height $V^{\rm max}_{\varphi\le\Lambda}$.

- The lower bound on r increases rapidly in the region $m_{\rm DM} \gtrsim 1.3\,{\rm TeV}$ due to the upper end of the parameter $m_t < 176\,{\rm GeV}$.

Actually, to realize the lowest bound $r \sim 10^{-5}$, the three-parameter tuning for m_t, $M_{\rm R}$, and $m_{\rm DM}$ is necessary. Some logic demanding the fine tuning such as MPP might realize these parameters.

In Fig. 6 (b), we plot for a wider range of the top-quark mass (127). The lower bound on r denoted by the black line increases in the region $m_{\rm DM} \gtrsim 1.3\,{\rm TeV}$ because of the difference of potential shapes; it will be explained in Sec. 4.6. The increasing in the region $m_{\rm DM} \gtrsim 1.5\,{\rm TeV}$ is due to the upper end of the parameter $m_t < 178\,{\rm GeV}$.

Let us see the implications of future discoveries. We will probably discover $m_{\rm DM}$ or r in near future earlier than the discovery of m_t or $M_{\rm R}$. Here, we fit $M_{\rm R}$ and m_t from the future observation of $m_{\rm DM}$ and r.[29]

[28] The plot will be shown in Sec. 4.5.3.

[29] Instead, if one narrow down the error on the top pole mass m_t e.g. at the High Luminosity LHC [80], one may use m_t and $m_{\rm DM}$ as input parameters to predict $M_{\rm R}$ and r.

- If we discover $m_{\rm DM} = 1\,{\rm TeV}$ ($\kappa \simeq 0.31$) and $r = 0.01$, the right-handed neutrino mass is predicted to be in the narrow range $10^{14}\,{\rm GeV} \lesssim M_{\rm R} \lesssim 10^{14.6}\,{\rm GeV}$ and the top-quark mass is constrained: $m_t < 174\,{\rm GeV}$.
- If we discover $m_{\rm DM} = 1.5\,{\rm TeV}$ ($\kappa \simeq 0.47$) and $r = 0.01$, we obtain the theoretical lower bound $M_{\rm R} \gtrsim 10^{14.6}\,{\rm GeV}$, while the top-quark mass is less constrained: $171\,{\rm GeV} < m_t < 178\,{\rm GeV}$. However, $M_{\rm R}$ and m_t are strongly correlated in this case. Therefore if one of them is fixed, the other is precisely predicted.

$m_{\rm DM}$	r	m_t	$M_{\rm R}$
$1\,{\rm TeV}$	0.01	$m_t < 174\,{\rm GeV}$	$10^{14}\,{\rm GeV} \lesssim M_{\rm R} \lesssim 10^{14.6}\,{\rm GeV}$
$1\,{\rm TeV}$	0.001	$173\,{\rm GeV} < m_t < 174\,{\rm GeV}$	$10^{14.1}\,{\rm GeV} \lesssim M_{\rm R} \lesssim 10^{14.3}\,{\rm GeV}$
$1.5\,{\rm TeV}$	0.01	$170\,{\rm GeV} < m_t < 178\,{\rm GeV}$	$10^{14.6}\,{\rm GeV} \lesssim M_{\rm R} \lesssim 10^{14.8}\,{\rm GeV}$
$1.5\,{\rm TeV}$	0.001	$m_t \simeq 177.8\,{\rm GeV}$	$M_{\rm R} \simeq 10^{14.6}\,{\rm GeV}$

Table 4: Constraints possibly obtained from future observations of $m_{\rm DM}$ and r for Normal Hierarchy.

See Table 4 for other pairs of $m_{\rm DM}$ and r. Generically the heavy dark-matter mass tends to predict the heavy top-quark mass and $M_{\rm R}$. The smaller the r is, the tighter the range of m_t. Especially, if we discover $m_{\rm DM} = 1.5\,{\rm TeV}$ and $r = 0.001$, m_t and $M_{\rm R}$ are accurately predicted.

We can predict $r_{\rm bound}$ or $m_{\rm DM}$ to some extent by considering typical input parameters. When we choose $m_t = 173\,{\rm GeV}$ and $M_{\rm R} = 10^{14}\,{\rm GeV}$, we obtain the bound $m_{\rm DM} \sim 860\,{\rm GeV}$–$970\,{\rm GeV}$ for $r < 0.09$.

Inverted Hierarchy We show the results for the case of Inverted Hierarchy ($n_\nu = 2$) in Figs. 7 and 8.

The right-handed neutrinos lighter than $\sim 10^{13}\,{\rm GeV}$ do not affect the analysis, similarly as in the case of Normal Hierarchy. However, the upper bound on $M_{\rm R}$ is slightly different: $M_{\rm R} \lesssim 10^{14.7}\,{\rm GeV}$.

Table 5 is the summary of prediction from future discoveries of the dark matter and r. Although we cannot obtain the global narrow bounds on $M_{\rm R}$ and m_t, they are highly correlated as in the case of Normal Hierarchy if we discover $m_{\rm DM} = 1.5\,{\rm TeV}$ and $r = 0.01$.

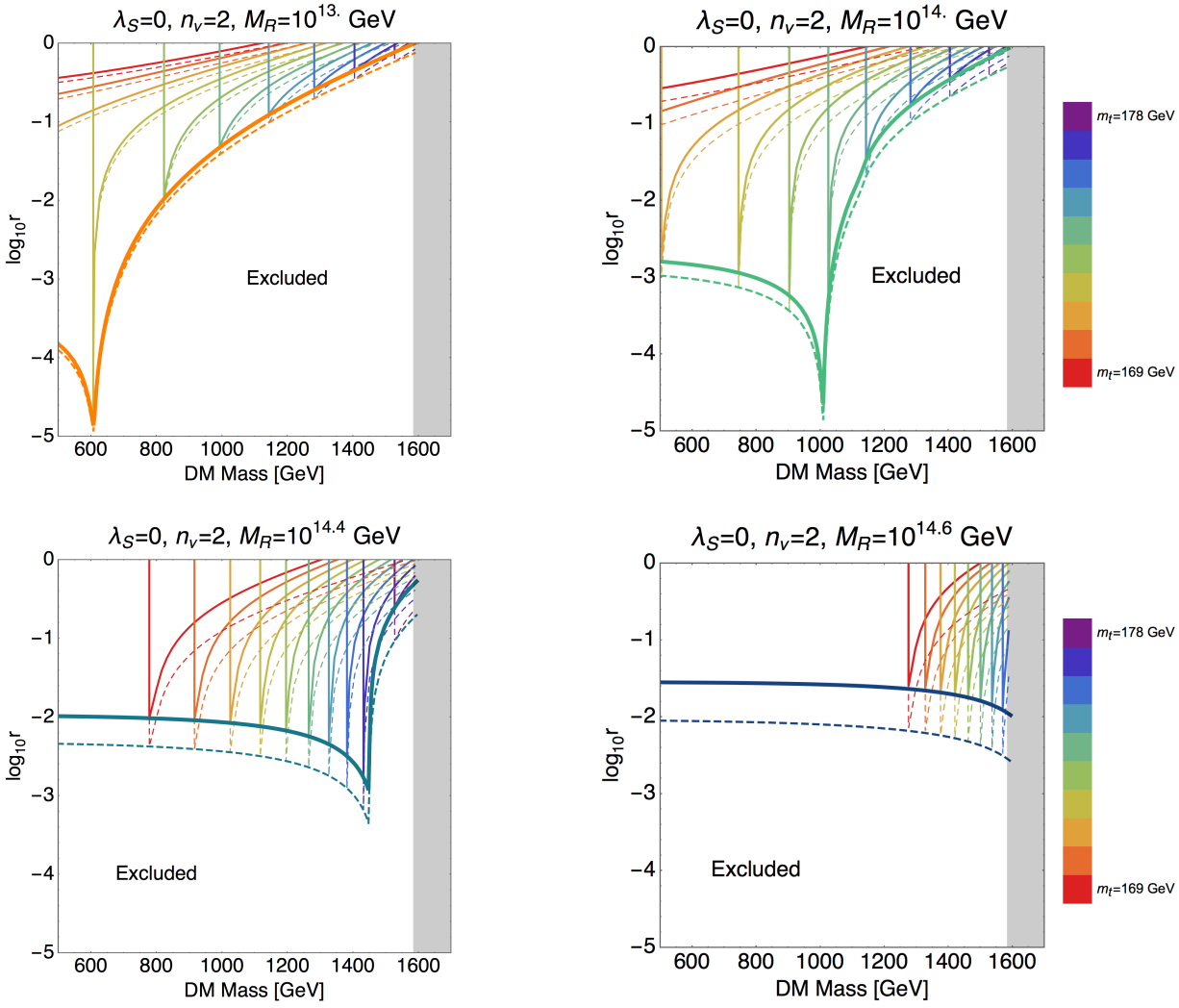

Figure 7: Allowed region for Inverted Hierarchy with $\lambda_S = 0$.

$m_{\rm DM}$	r	m_t	$M_{\rm R}$
1 TeV	0.01	$m_t < 174\,\text{GeV}$	$10^{13.9}\,\text{GeV} \lesssim M_{\rm R} < 10^{14.5}\,\text{GeV}$
1 TeV	0.001	$173\,\text{GeV} < m_t < 174\,\text{GeV}$	$10^{13.9}\,\text{GeV} < M_{\rm R} < 10^{14.2}\,\text{GeV}$
1.5 TeV	0.01	$m_t < 178\,\text{GeV}$	$10^{14.4}\,\text{GeV} < M_{\rm R} \lesssim 10^{14.7}\,\text{GeV}$
1.5 TeV	0.001	$177\,\text{GeV} < m_t < 178\,\text{GeV}$	$10^{14.4}\,\text{GeV} < M_{\rm R} < 10^{14.5}\,\text{GeV}$

Table 5: Constraints possibly obtained from future observations of $m_{\rm DM}$ and r for Inverted Hierarchy.

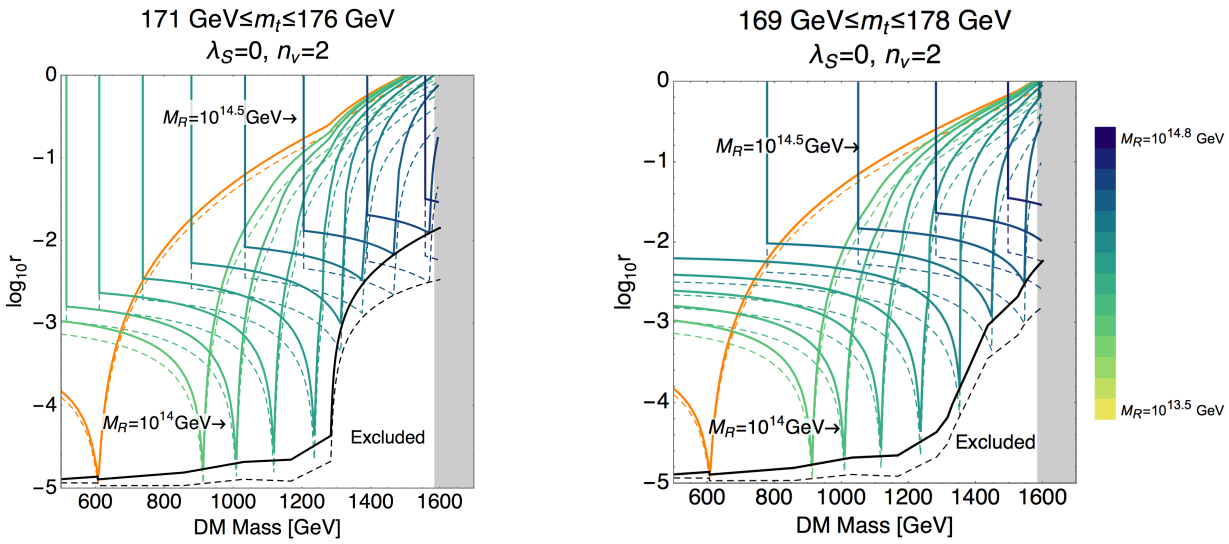

(a) (b)

Figure 8: The allowed region for Inverted Hierarchy.
(a) The lower bound on r for each fixed $M_{\rm R}$ (colored) and their envelope (black) with $\lambda_S = 0$ and $171\,{\rm GeV} < m_t < 176\,{\rm GeV}$. The orange line is for $M_{\rm R} = 10^{13}$ GeV. The vertical colored line comes from the lower end, $m_t > 171\,{\rm GeV}$.
(b) The same plot for $\lambda_S = 0$ and $169\,{\rm GeV} < m_t < 178\,{\rm GeV}$.

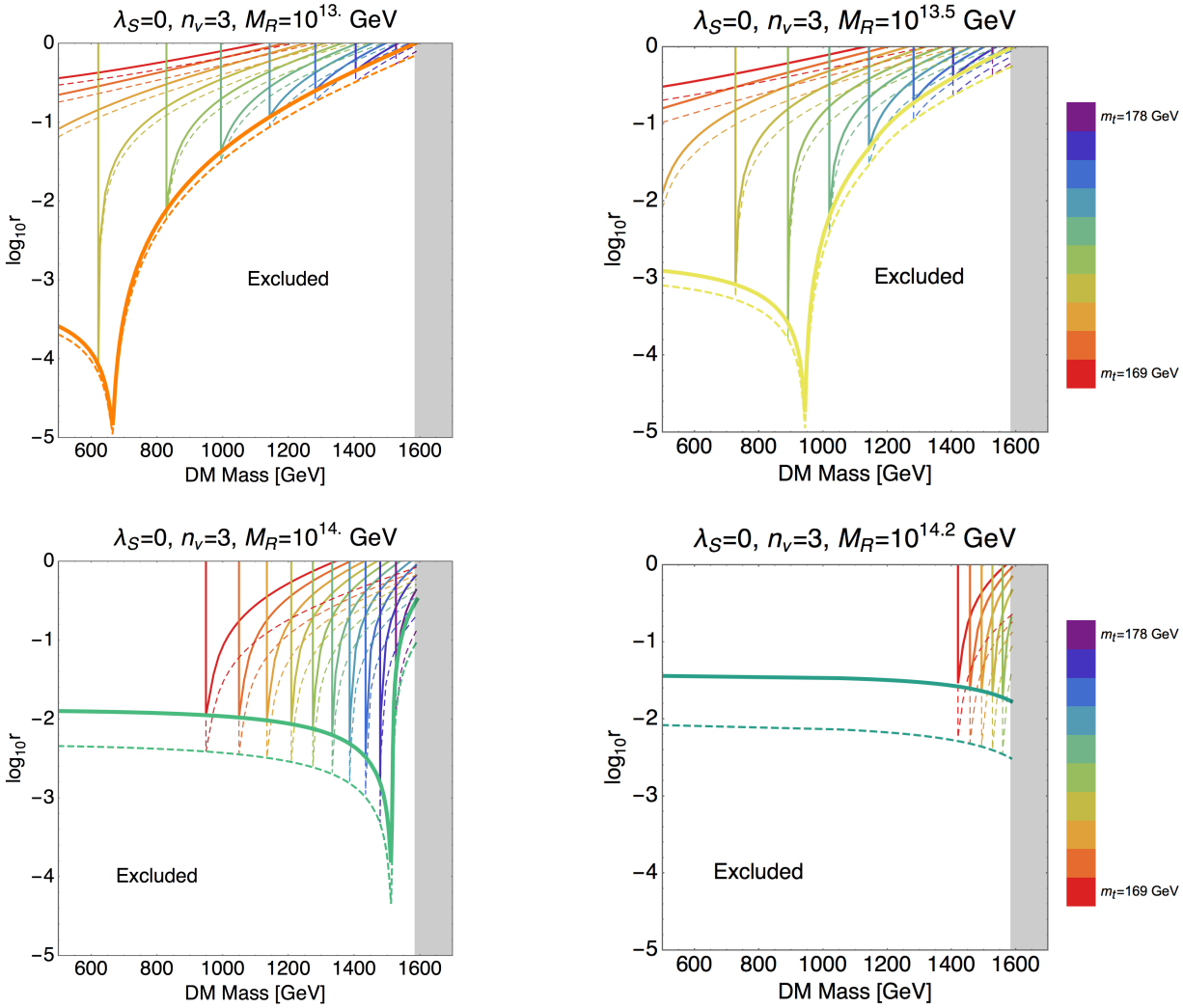

Figure 9: Allowed region for Degenerate case with $\lambda_S = 0$.

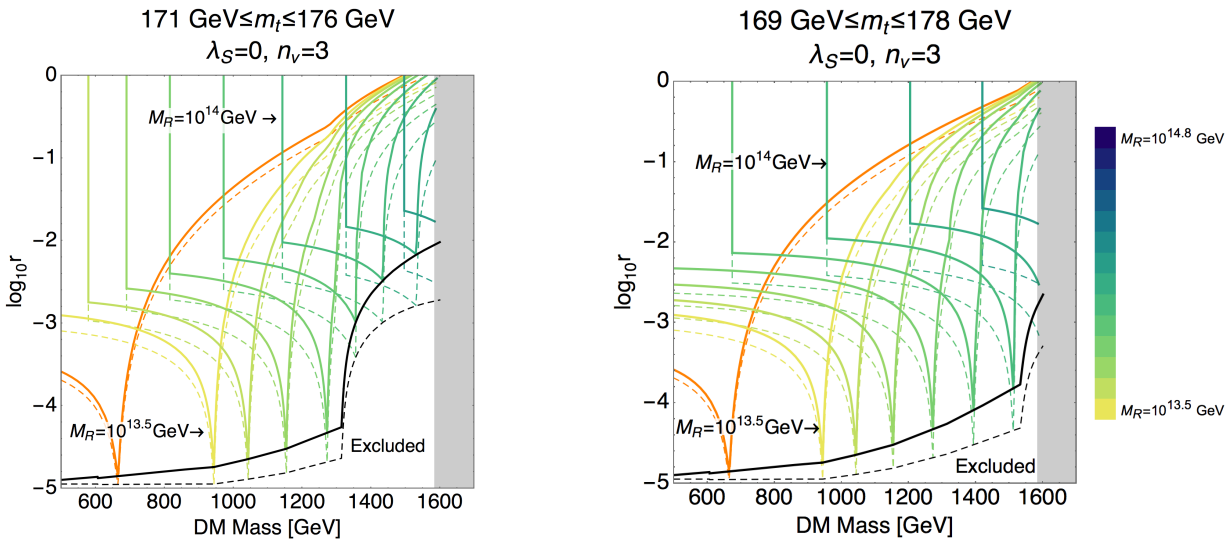

(a) (b)

Figure 10: The allowed region for Degenerate case.
(a) The lower bound on r for each fixed $M_{\rm R}$ (colored) and their envelope (black) with $\lambda_S = 0$ and $171\,{\rm GeV} < m_t < 176\,{\rm GeV}$. The orange line is for $M_{\rm R} = 10^{13}$ GeV. The vertical colored line comes from the lower end, $m_t > 171\,{\rm GeV}$.
(b) The same plot for $\lambda_S = 0$ and $169\,{\rm GeV} < m_t < 178\,{\rm GeV}$.

Degenerate case We show the results for Degenerated case ($n_\nu = 3$) in Fig. 9.

The right-handed neutrinos lighter than $\sim 10^{13}\,\mathrm{GeV}$ do not affect the analysis, similarly as other cases. On the other hand, the upper bound on M_R becomes smaller than in other cases: $M_\mathrm{R} \lesssim 10^{14.2}\,\mathrm{GeV} \simeq 1.6 \times 10^{14}\,\mathrm{GeV}$.

We summarize implications of future discoveries m_DM and r in Table 6. The right-handed neutrino mass tend to be lighter than hierarchical cases due to the heavy m_ν. However, the prediction of m_t is similar to the other cases.

m_DM	r	m_t	M_R
1 TeV	0.01	$m_t < 174\,\mathrm{GeV}$	$10^{13.5}\,\mathrm{GeV} \lesssim M_\mathrm{R} \lesssim 10^{14}\,\mathrm{GeV}$
1 TeV	0.001	$173\,\mathrm{GeV} \lesssim m_t < 174\,\mathrm{GeV}$	$10^{13.5}\,\mathrm{GeV} < M_\mathrm{R} < 10^{13.8}\,\mathrm{GeV}$
1.5 TeV	0.01	$m_t < 178\,\mathrm{GeV}$	$10^{14}\,\mathrm{GeV} \lesssim M_\mathrm{R} \lesssim 10^{14.2}\,\mathrm{GeV}$
1.5 TeV	0.001	$176\,\mathrm{GeV} < m_t < 178\,\mathrm{GeV}$	$M_\mathrm{R} \simeq 10^{14}\,\mathrm{GeV}$

Table 6: Constraints obtained for degenerate case.

4.5.3 Lower bound on r for each m_t

In this section, let us temporarily forgot the top-quark-mass ranges Eqs. (126) and (127). In Fig. 11, we show the lower bound on r for each fixed m_t with $M_{\rm R}$ being varied. The black envelope lines in Fig. 11 are identical to the ones in Sec. 4.5.2 except for their right-most boundary where they follow the $m_t = 176\,\text{GeV}$ (blue) line or $178\,\text{GeV}$ (purple) line.

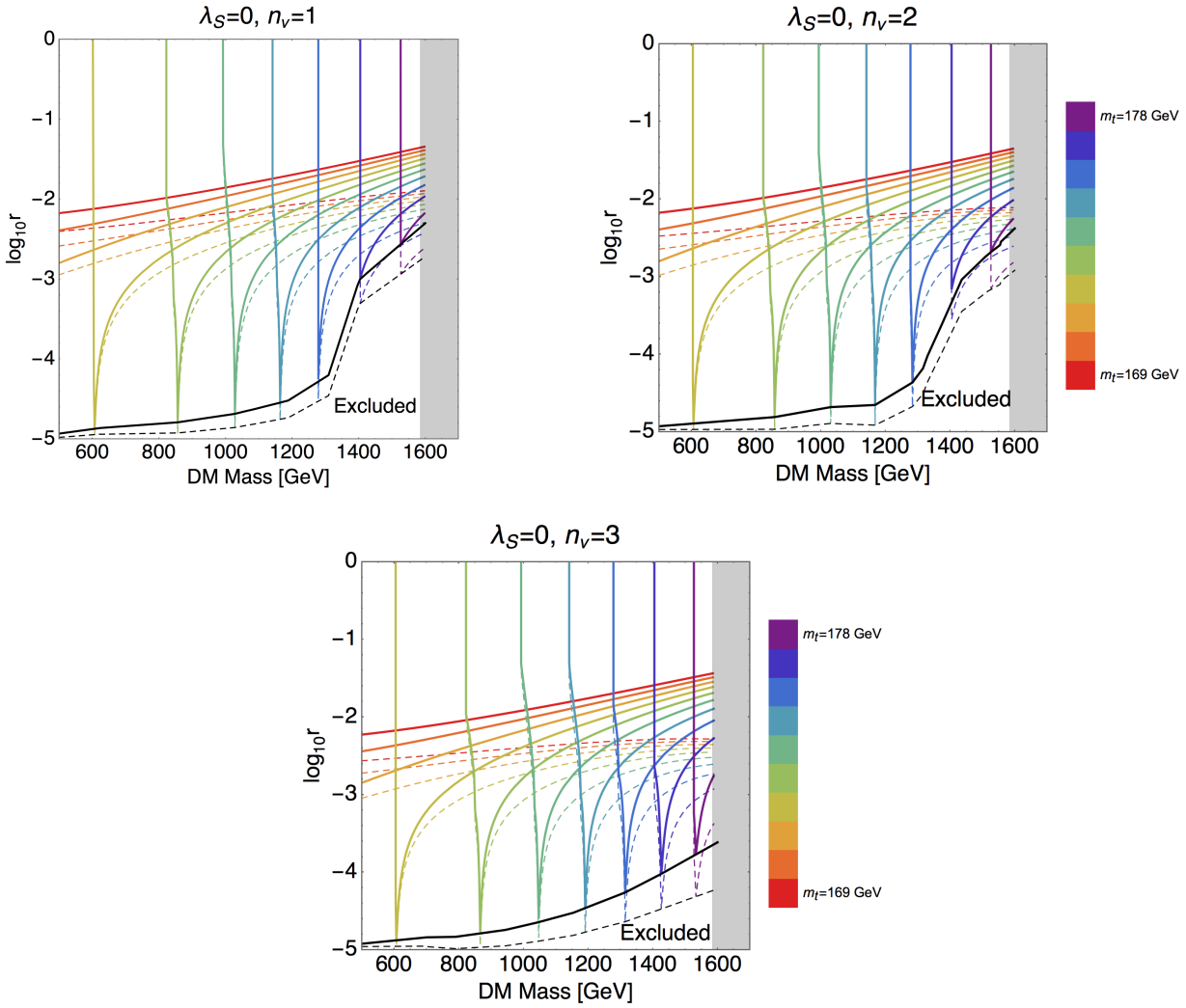

Figure 11: The lower bound on r for each fixed m_t with $\lambda_S = 0$. See the left of Fig. 3 (a) for the corresponding plot without right-handed neutrinos.

We see that there is the upper bound on m_t for a given $m_{\rm DM}$ and it hardly depends on n_ν. In other words, if any lower bound on m_t is given, we obtain the lower bound of $m_{\rm DM}$ without any assumptions on the other parameters in the neutrino sector. Also we see that there is a strong correlation between m_t and $m_{\rm DM}$ regardless of n_ν if $r < 10^{-3}$.

For example, if we discover $r = 10^{-3}$ and $m_{\rm DM} = 1\,\text{TeV}$ in the future, m_t must be between 173 GeV and 174 GeV.

4.6 The form of envelope by potential shape

In this section, we explain the shape of envelopes denoted by the black or colored-thick line in the figures.

First, we start with the case without heavy right-handed neutrino (Fig. 3 (a)). In this case, the effective Higgs potential generally has one local minimum due to the top-quark loop correction.[30] At the minimum point of envelope, the maximum value of the Higgs potential becomes smallest compared with the one which is obtained by another set of parameters.

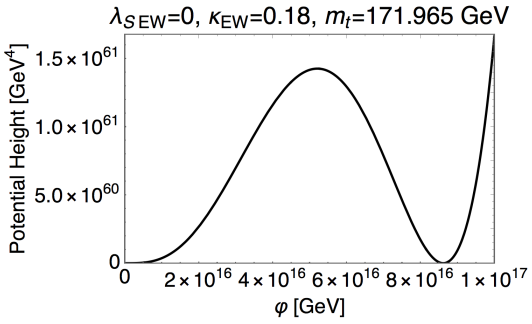

Figure 12: The shape of Higgs potential with the values of m_t and $m_{\rm DM}$ (κ) that corresponds to a point near the minimum of the envelope in Fig. 3 (a).

In Fig. 12, we show the shape of potential near this point. At this minimum point, the height at the local maximum (at $\varphi \simeq 5 \times 10^{16}\,\text{GeV}$ in the case of Fig. 12) becomes equal to the height at $\varphi = \Lambda$. If the local potential minimum (at $\varphi \simeq 9 \times 10^{16}\,\text{GeV}$ in the case of Fig. 12) is moved left, the height at $\varphi = \Lambda$ becomes larger; on the other hand if it is moved right, the height at the local maximum becomes larger. The left curve of the minimum point of the envelope in Fig. 3 (a) is governed by the local maximum of the potential, while the right by the value at $\varphi = \Lambda$.

Second we consider the case with right-handed neutrinos. The envelope denoted by the colored thick line in Figs. 5, 7, and 9 also have the minimal points. Actually there is one more (hardly visible) discontinuity in each envelope[31] because the Higgs potential

[30] Here we let the word "minimum" also stands for mere a concavity.

[31] They can be seen a little bit easily in Figs. 6, 8 and 10, where the envelopes are summarized in a single panel with the same colors. The discontinuity is located, e.g. in the $n_\nu = 1$ case (Fig. 6), at $(m_{\rm DM}, \log_{10} r) \sim (1050\,\text{GeV}, -1.5)$ for $M_{\rm R} = 10^{14}\,\text{GeV}$, $(1100\,\text{GeV}, -1.7)$ for $M_{\rm R} = 10^{14.1}\,\text{GeV}$, $(1150\,\text{GeV}, -2)$ for $M_{\rm R} = 10^{14.2}\,\text{GeV}$, and $(1220\,\text{GeV}, -2.6)$ for $M_{\rm R} = 10^{14.3}\,\text{GeV}$.

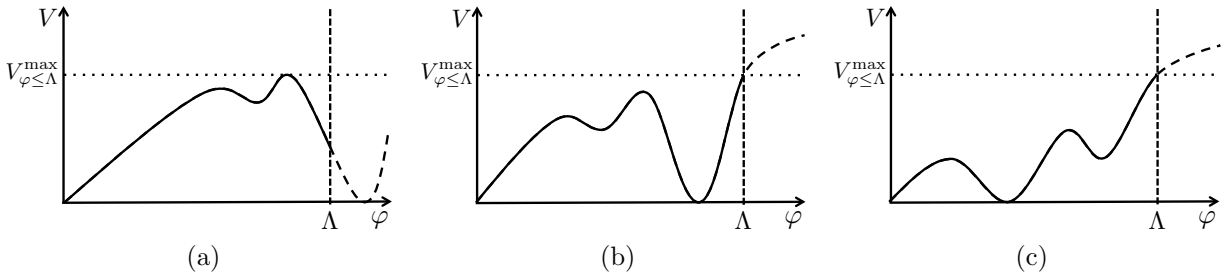

Figure 13: Schematic potential shapes. (a) Typical potential shape when its minimum is at $\varphi > \Lambda$. (b) Typical potential shape when the minimum at larger φ gives lower height. (c) Typical potential shape when the minimum at smaller φ gives lower height.

has the second local minimum due to the neutrino in general. The additional minimum is located at higher scale than the one of top-quark. Thus there are the following three kinds of potential shapes:

(i) The potential minimum at higher φ is located at $\varphi > \Lambda$ (Fig. 13 (a)). This corresponds to the left side of the minimum of each envelope.

(ii) There are two potential minima and the height of the one at larger φ is smaller (Fig. 13 (b)). This corresponds to the region between the minimum and the discontinuity of each envelope.

(iii) There are two potential minima and the height of the one at lower φ is smaller (Fig. 13 (c)). This corresponds to the right side of the discontinuity of each envelope.

From this approach, the black lines in Figs. 6, 8 and 10 are understand as the parametric lines where the two potential minima are degenerate.

We can see the additional discontinuity from another point of view in Fig. 14. The left end of each solid rainbow-colored line should touch the black lower-bound line for $n_\nu = 0$ because there usually corresponds to $M_{\rm R} \to 0$ limit in usual. However, they do not touch the black $n_\nu = 0$ line for $m_t \gtrsim 175\,\text{GeV}$. This is because there arises the two local minima of the potential as in the case (iii): The minimum at lower φ by the top-quark contribution is tuned to be zero, while the minimum at higher φ by the neutrino contribution can reduce the maximum potential height freely. The gray line in Fig. 14 links the left ends of the solid rainbow-colored lines for the region $m_t \gtrsim 175\,\text{GeV}$, and is the same as the line joining the discontinuities mentioned above.

Finally, we explain why the envelope in Figs. 6 (b) and 8 (b) (black, lower) is bent in the large $m_{\rm DM}$ region. At the point where the gray line touches the black envelope, the potential height of the two degenerate minima becomes zero and the higher one is at $\varphi = \Lambda$.

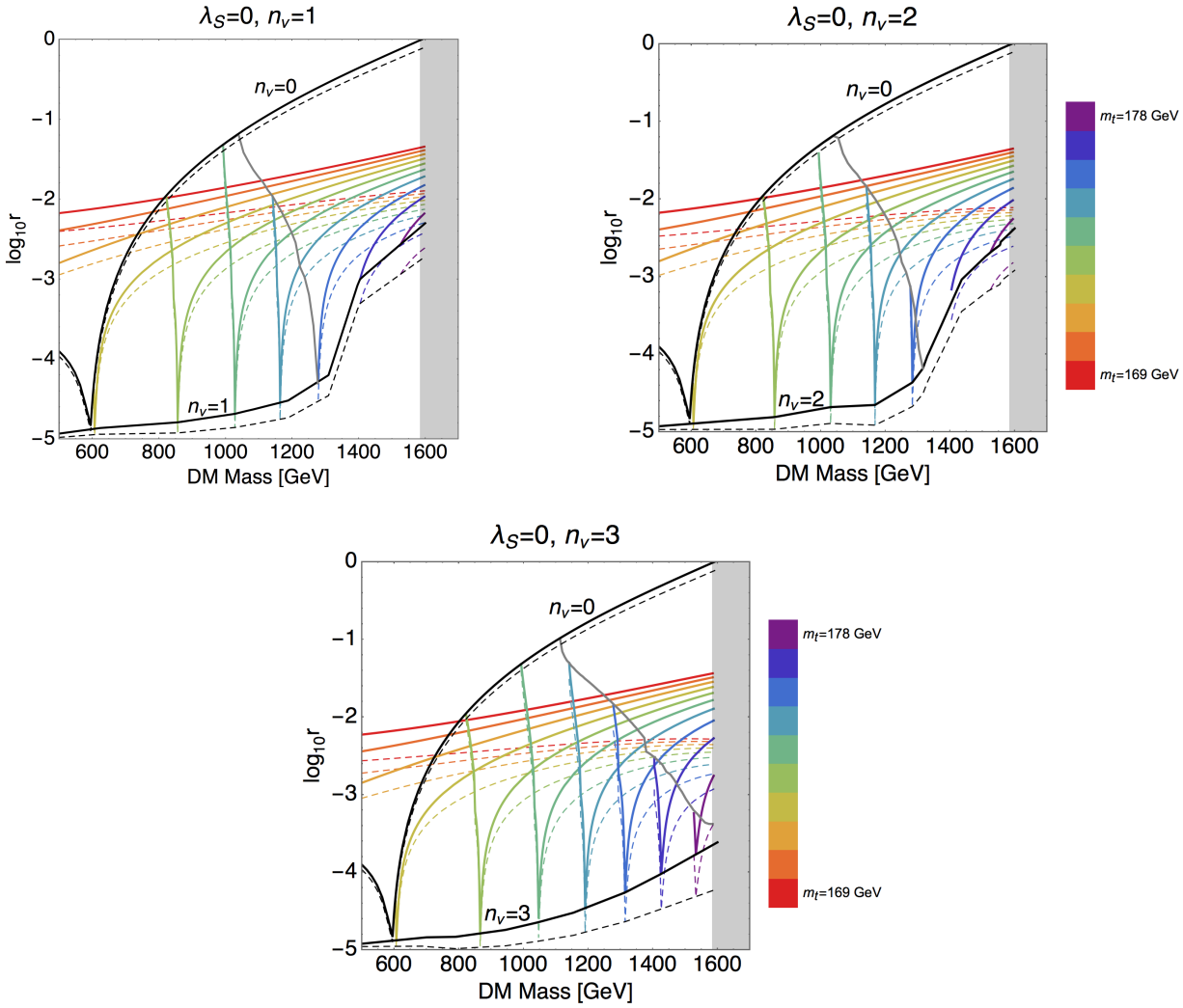

Figure 14: The same plot as in Fig. 11. The black $n_\nu = 0$ line in Fig. 3 is also superimposed. The gray line show the location of the discontinuity explained in the text, and links the left ends of the rainbow-colored lines for $m_t \gtrsim 175\,\mathrm{GeV}$.

On its right side, the case (i) is realized, and the maximum potential height becomes much larger than the cases (ii) and (iii) with the two minima. At this point, the electroweak vacuum and these two vacua are all degenerate to (nearly) zero, and the vacuum with highest φ is located at $\varphi = \Lambda$. This point may be interesting in term of the MPP, but we do not investigate it anymore in this thesis.

4.7 Summary of results

Finally we summarize the results in this section.

We have analyzed the effective Higgs potential of the Higgs-portal Z_2 scalar model (120). The current observational constraints on the tensor-to-scalar ratio and the dark-matter mass are $r \leq 0.09$ [6] and $m_{\rm DM} \gtrsim 1\,{\rm TeV}$ [70], respectively. We set the cutoff scale Λ of the low-energy effective theory as $\Lambda = 10^{17}\,{\rm GeV}$.

First, there is the universal upper bound on $m_{\rm DM}$ due to the Landau pole:

$$m_{\rm DM} \lesssim 1.6\,{\rm TeV}. \tag{139}$$

This bound hardly depends on Λ and mass of right-handed neutrino.

In the case without the heavy right-handed neutrinos, we have obtained the theoretical bounds

$$r \gtrsim 4 \times 10^{-2}, \tag{140}$$

$$m_{\rm DM} \lesssim 1.1\,{\rm TeV}, \tag{141}$$

$$174\,{\rm GeV} < m_t < 175\,{\rm GeV} \tag{142}$$

for the current observational constraints. The bound on $m_{\rm DM}$ is stringent than the bound by the Landau pole, and the allowed range of m_t is narrow. We may verify whether this inflation model is realistic by future experiments.

With the heavy right-handed neutrinos, we obtain the wider allowed region in the r-$m_{\rm DM}$ plane. If we allow a three-parameter (m_t, $M_{\rm R}$, and κ) tuning, we obtain

$$r \gtrsim 10^{-5}. \tag{143}$$

In this case the upper bound on dark-matter mass is determined by the Landau pole. Although the region $r \lesssim 10^{-3}$ is hard to see for the planned near-future observations, the region to explore may be shrunken by the combination with the accelerator experiments because there are the strong correlations between m_t, $m_{\rm DM}$ and the right-handed neutrino mass $M_{\rm R}$. Moreover, when we restrict $m_{\rm DM} \gtrsim 1.3\,{\rm TeV}$, we obtain a stronger bound $r \gtrsim 10^{-3}$ for a reasonable top-quark mass range.

5 Conclusion

We have discussed the following two themes related to the Higgs inflation with nonminimal couplings:

- What the difference of the prescription is.
- How the lower bound on r is obtained without the detailed knowledge of inflation mechanism.

On the first theme, we have shown the frame invariance of the one-loop effective action in the simplified Higgs-Yukawa model. Though the change of the path integral measure causes the difference between the Jordan frame and the Einstein frame, it can be absorbed by the counterterms because it is quartic divergent. If we properly take into account the change of path integral measure, the effective actions are exactly the same regardless of frame where we calculate it.

However there is still the difference of predictions between the two prescriptions I and II. We have pointed out that the difference can be absorbed into the choice of tree-level potential from infinitely many possibilities: The prescriptions I and II are merely two specific choices of tree-level potential, and the difference may appears in the higher dimensional terms. We have also proposed a mechanism to stop the running of the effective quartic coupling in the prescription II in the ordinary context, using the gauge kinetic function.

On the second theme, we have analyzed the Higgs-portal Z_2 scalar dark-matter model and obtained the lower bound on the tensor-to-scalar ratio r and the upper bound on the dark-matter mass m_{DM}. The advantage of our approach is that we can obtain the lower bound on r without knowing any detail of the high-scale physics. Under the assumption that the extrapolation of the Higgs-field direction plays the role of inflaton at $\varphi > \Lambda$, the lower bounds on r are appeared in the region we may observe in near future in some cases. This analysis can be applied to other inflation model and we may check the feasibility of the model in the same way.

There are interesting topics to investigate. First, if the Higgs field is trapped at a false vacuum, a small scale inflation may occurs depending on the initial condition at the end of the main inflation. Second, the universe may have double or triple degenerate vacua in specific parameter sets as mentioned in Sec. 4.6. If the tensor-to-scalar ratio and the dark-matter mass point such a parameter set, it would be intriguing to reveal the mechanism that the parameters are naturally selected.

In this thesis, we regard the gravity is the background field and did not consider the renormalization of it. Of course this treatment is not enough to investigate the unified theory. There is also the possibility that the graviton-loop effect modifies the effective

Higgs potential and predicts different result. It would be worth to include the scalar-loop effect, as in Ref. [15], and also the one from gauge-boson loops.

Appendices

A Renormalization group equations

We show the RGEs and the way to calculate the lower bound on r. In this section, we omit the argument of the couplings: They are not the values at $\mu = m_t$ and they have the scale dependence in this Appendix.

We have calculated the lower bound on r as follows:

1. Solve the RGEs (147)–(154) for given parameters with the initial conditions for the SM parameters (155)–(159). (Equations will be shown in the end of this section.) The effects from right-handed neutrino is introduced only at high energy scale $\varphi \geq M_{\rm R}$: We set $n_\nu = 0$ and $M_{\rm R} = 0$ in $\varphi < M_{\rm R}$. As the boundary condition to solve the RGEs, we have used Eqs. (11)–(15) in [68] and the values in Table 7.

	Value	Reference
Planck mass $M_{\rm P}$	2.4353×10^{18} GeV	[72]
Higgs mass m_H	125.09 GeV	[25]
Z boson mass M_Z	91.1876 GeV	[72]
W boson mass M_W	80.384 GeV	See the caption
$\overline{\rm MS}$ strong coupling $\alpha_3(M_Z)$	0.1184	[33]
The expectation value of the Higgs field v	246 GeV	[72]

Table 7: Boundary condition for the RGEs. The recent value of M_W from Ref. [72] is $M_W = 80.385 \pm 0.015\,\text{GeV}$. The difference from the central value is smaller than the error and it causes smaller contribution ($\leq \mathcal{O}\left(10^{-5}\right)$) than the theoretical uncertainity.

2. Calculate the one-loop effective Higgs potential

$$V_{\varphi \leq \Lambda} = \frac{\lambda_{\rm eff}}{4}\varphi^4 \tag{144}$$

where

$$\lambda_{\rm eff} := e^{4\Gamma}\left[\lambda + \frac{1}{16\pi^2}\left\{ -3y_t^4\left(\ln\frac{y_t^2}{2} - \frac{3}{2} + 2\Gamma\right) + \frac{3g_2^2}{8}\left(\ln\frac{g_2^2}{4} - \frac{5}{6} + 2\Gamma\right) \right.\right.$$
$$+ \frac{3(g_Y^2+g_2^2)^2}{16}\left(\ln\frac{g_Y^2+g_2^2}{4} - \frac{5}{6} + 2\Gamma\right)$$
$$\left.\left. - n_\nu y_\nu^4 \ln\left(\frac{M_{\rm R} + \sqrt{M_{\rm R}^2 + 4y_\nu^2\varphi^2}}{2\sqrt{M_{\rm R}^2+\varphi^2}}\right)\right\}\right] \tag{145}$$

is the effective Higgs-self coupling. Here we introduce the last term in the braces which is introduced to naively take into account the effect of the neutrino loop on the effective potential.[32] We set $\mu = \varphi$ when we calculate $\lambda_{\rm eff}$;[33] see [24] for the treatment of the renormalization scale μ of $\lambda_{\rm eff}$. Here we neglect the one-loop wave-function renormalization

$$\Gamma(\varphi) = \int_{m_t}^{\varphi} \frac{1}{16\pi^2}\left(\frac{9}{4}g_2^2 + \frac{3}{4}g_Y^2 - 3y_t^2 - n_\nu y_\nu^2\right) {\rm d}\ln\mu \tag{146}$$

due to the calculation cost and we will estimate its error later.

3. Change the parameters using the false position method until the value of the potential minimum becomes sufficiently close to zero.

4. Calculate the maximum value of potential and obtain $r_{\rm bound}$ via Eq. (119).

5. Obtain the value of $\Gamma(\varphi)$ at $\varphi = \Lambda$ and use it to estimate the deviation at the potential maximum: We calculate the coeffient factor $\exp(4\Gamma(\Lambda))$. This is most conservative because $|\Gamma(\varphi)|$ becomes largest at $\varphi = \Lambda$. This estimation corresponding to the dashed lines in the figures.

[32] We checked that its effect is at most few percent.

[33] That is, we implicitly assume the tree-level potential is defined as Eq. (96) with the counterterm (80), as explained in Sec. 3.5.

Renormalization group equations We obtained the RGEs for arbitrary n_ν by combining the $n_\nu = 1$ RGEs [81] and the $n_\nu = 3$ ones [82]:

$$\frac{\mathrm{d}g_Y}{\mathrm{d}\ln\mu} = \frac{1}{16\pi^2}\frac{41}{6}g_Y^3 + \frac{g_Y^3}{(16\pi^2)^2}\left(\frac{199}{18}g_Y^2 + \frac{9}{2}g_2^2 + \frac{44}{3}g_3^2 - \frac{17}{6}y_t^2 - \frac{n_\nu}{2}y_\nu^2\right), \tag{147}$$

$$\frac{\mathrm{d}g_2}{\mathrm{d}\ln\mu} = -\frac{1}{16\pi^2}\frac{19}{6}g_2^3 + \frac{g_2^3}{(16\pi^2)^2}\left(\frac{3}{2}g_Y^2 + \frac{35}{6}g_2^2 + 12g_3^2 - \frac{3}{2}y_t^2 - \frac{n_\nu}{2}y_\nu^2\right), \tag{148}$$

$$\frac{\mathrm{d}g_3}{\mathrm{d}\ln\mu} = -\frac{7}{16\pi^2}g_3^3 + \frac{g_3^3}{(16\pi^2)^2}\left(\frac{11}{6}g_Y^2 + \frac{9}{2}g_2^2 - 26g_3^2 - 2y_t^2\right), \tag{149}$$

$$\begin{aligned}\frac{\mathrm{d}y_t}{\mathrm{d}\ln\mu} = {}& \frac{y_t}{16\pi^2}\left(\frac{9}{2}y_t^2 + n_\nu y_\nu^2 - \frac{17}{12}g_Y^2 - \frac{9}{4}g_2^2 - 8g_3^2\right)\\ &+ \frac{y_t}{(16\pi^2)^2}\Bigg\{-12y_t^2 - \frac{9n_\nu}{4}y_\nu^4 - \frac{9n_\nu}{4}y_t^2y_\nu^2 + 6\lambda^2 + \frac{1}{4}\kappa^2 - 12\lambda y_t^2\\ &\qquad + g_Y^2\left(\frac{131}{16}y_t^2 + \frac{5n_\nu}{8}y_\nu^2\right) + g_2^2\left(\frac{225}{16}y_t^2 + \frac{5n_\nu}{8}y_\nu^2\right) + 36g_3^2y_t^2\\ &\qquad + \frac{1187}{216}g_Y^4 - \frac{23}{4}g_2^4 - 108g_3^4 - \frac{3}{4}g_Y^2g_2^2 + 9g_2^2g_3^2 + \frac{19}{9}g_3^2g_Y^2\Bigg\},\end{aligned} \tag{150}$$

$$\begin{aligned}\frac{\mathrm{d}y_\nu}{\mathrm{d}\ln\mu} = {}& \frac{y_\nu}{16\pi^2}\left\{\left(n_\nu + \frac{3}{2}\right)y_\nu^2 + 3y_t^2 - \frac{3}{4}g_Y^2 - \frac{9}{4}g_2^2\right\}\\ &+ \frac{y_\nu}{(16\pi^2)^2}\Bigg[-\left(\frac{9n_\nu}{2} - \frac{3}{2}\right)y_\nu^4 - \frac{27}{4}y_t^4 - \frac{27}{4}y_t^2y_\nu^2 + 6\lambda^2 + \frac{1}{4}\kappa^2 - 12\lambda y_\nu^2\\ &\qquad + g_Y^2\left\{\left(\frac{5n_\nu}{8} + \frac{93}{16}\right)y_\nu^2 + \frac{85}{24}y_t^2\right\} + g_2^2\left\{\left(\frac{15n_\nu}{8} + \frac{135}{16}\right)y_\nu^2 + \frac{45}{8}y_t^2\right\}\\ &\qquad + 20g_3^2y_t^2 + \frac{35}{24}g_Y^4 - \frac{23}{4}g_2^4 - \frac{9}{4}g_Y^2g_2^2\Bigg],\end{aligned} \tag{151}$$

$$\begin{aligned}\frac{\mathrm{d}\lambda}{\mathrm{d}\ln\mu} = {}& \frac{1}{16\pi^2}\left(\frac{1}{2}\kappa^2 + 24\lambda^2 - 3g_Y^2\lambda - 9g_2^2\lambda + 4n_\nu\lambda y_\nu^2\right.\\ &\qquad \left. + \frac{3}{8}g_Y^4 + \frac{3}{4}g_Y^2g_2^2 + \frac{9}{8}g_2^4 + 12\lambda y_t^2 - 6y_t^4 - 2n_\nu y_\nu^4\right)\\ &+ \frac{1}{(16\pi^2)^2}\Bigg\{-2\kappa^3 - 5\kappa^2\lambda - 312\lambda^3 + 36\lambda^2(g_Y^2 + 3g_2^2) + \lambda y_\nu^2\left(\frac{5n_\nu}{2}g_Y^2 + \frac{15n_\nu}{2}g_2^2\right)\\ &\qquad - \lambda\left(\frac{629}{24}g_Y^4 - \frac{39}{4}g_Y^2g_2^2 + \frac{73}{8}g_2^4\right) + \lambda y_t^2\left(\frac{85}{6}g_Y^2 + \frac{45}{2}g_2^2 + 80g_3^2\right)\\ &\qquad + \frac{305}{16}g_2^6 - \frac{289}{48}g_Y^2g_2^4 - \frac{559}{48}g_Y^4g_2^2 - \frac{379}{48}g_Y^6 - 32g_3^2y_t^4 - \frac{8}{3}g_Y^2y_t^4\\ &\qquad - \frac{9}{4}g_2^4y_t^2 - \frac{3n_\nu}{4}g_2^4y_\nu^2 + g_Y^2y_t^2\left(-\frac{19}{4}g_Y^2 + \frac{21}{2}g_2^2\right) - g_Y^2y_\nu^2\left(\frac{n_\nu}{4}g_Y^2 + \frac{n_\nu}{2}g_2^2\right)\\ &\qquad - 144\lambda^2y_t^2 - 48n_\nu y_\nu^2 - 3\lambda y_t^4 - n_\nu\lambda y_\nu^4 + 30y_t^6 + 10n_\nu y_\nu^6\Bigg\},\end{aligned} \tag{152}$$

$$\frac{\mathrm{d}\kappa}{\mathrm{d}\ln\mu} = \frac{\kappa}{16\pi^2}\left(12\lambda + \lambda_S + 4\kappa + 6y_t^2 + 2n_\nu y_\nu^2 - \frac{3}{2}g_Y^2 - \frac{9}{2}g_2^2\right)$$
$$+ \frac{\kappa}{(16\pi^2)^2}\Bigg\{ - \frac{21}{2}\kappa^2 - 72\kappa\lambda - 60\lambda^2 - 6\kappa\lambda_S - \frac{5}{6}\lambda_S^2 - y_t^2(12\kappa + 72\lambda) - 4n_\nu\kappa y_\nu^2$$
$$- 24n_\nu\lambda y_\nu^2 - \frac{27}{2}y_t^4 - \frac{9n_\nu}{2}y_\nu^4 + g_Y^2(\kappa + 24\lambda) + g_2^2(3\kappa + 72\lambda)$$
$$+ y_t^2\left(\frac{85}{12}g_Y^2 + \frac{45}{4}g_2^2 + 40g_3^2\right) + y_\nu^2\left(\frac{5n_\nu}{4}g_Y^2 + \frac{15n_\nu}{4}g_2^2\right)$$
$$+ \frac{557}{48}g_Y^4 - \frac{145}{16}g_2^4 + \frac{15}{8}g_Y^2 g_2^2\Bigg\}, \tag{153}$$

$$\frac{\mathrm{d}\lambda_S}{\mathrm{d}\ln\mu} = \frac{1}{16\pi^2}\left(3\lambda_S^2 + 12\kappa^2\right)$$
$$+ \frac{1}{(16\pi^2)^2}\Bigg\{ - \frac{17}{3}\lambda_S^3 - 20\kappa^2\lambda_S - 48\kappa^3 + 24\kappa^2\left(-3y_t^2 - n_\nu y_\nu^2 + g_Y^2 + 3g_2^2\right)\Bigg\}. \tag{154}$$

Initial conditions for the SM parameters We show the relations between the SM parameters and the pole mass of top quark at two-loop level. These relations are given in Ref. [33].

$$g_Y(m_t) = 0.35761 + 0.00011\left(\frac{m_t}{\mathrm{GeV}} - 173.10\right) - 0.00021\left(\frac{M_W - 80.384\,\mathrm{GeV}}{0.014\,\mathrm{GeV}}\right) \tag{155}$$

$$g_2(m_t) = 0.64822 + 0.00004\left(\frac{m_t}{\mathrm{GeV}} - 173.10\right) + 0.00011\left(\frac{M_W - 80.384\,\mathrm{GeV}}{0.014\,\mathrm{GeV}}\right) \tag{156}$$

$$g_3(m_t) = 1.1666 - 0.00046\left(\frac{m_t}{\mathrm{GeV}} - 173.10\right) + 0.00314\left(\frac{\alpha_3(M_Z) - 0.1184}{0.0007}\right) \tag{157}$$

$$y_t(m_t) = 0.93558 + 0.00550\left(\frac{m_t}{\mathrm{GeV}} - 173.10\right) - 0.00042\left(\frac{\alpha_3(M_Z) - 0.1184}{0.0007}\right)$$
$$- 0.00042\left(\frac{M_W - 80.384\,\mathrm{GeV}}{0.014\,\mathrm{GeV}}\right) \tag{158}$$

$$\lambda(m_t) = 0.12711 + 0.00206\left(\frac{m_H}{\mathrm{GeV}} - 125.66\right) - 0.00004\left(\frac{m_t}{\mathrm{GeV}} - 173.10\right) \tag{159}$$

References

[1] A. A. Starobinsky, *Spectrum of relict gravitational radiation and the early state of the universe*, JETP Lett. **30** (1979), 682–685, [Pisma Zh. Eksp. Teor. Fiz.30,719(1979)].

[2] A. H. Guth, *The Inflationary Universe: A Possible Solution to the Horizon and Flatness Problems*, Phys. Rev. **D23** (1981), 347–356.

[3] K. Sato, *First Order Phase Transition of a Vacuum and Expansion of the Universe*, Mon. Not. Roy. Astron. Soc. **195** (1981), 467–479.

[4] A. D. Linde, *A New Inflationary Universe Scenario: A Possible Solution of the Horizon, Flatness, Homogeneity, Isotropy and Primordial Monopole Problems*, Phys. Lett. **108B** (1982), 389–393.

[5] Virgo, LIGO Scientific, B. P. Abbott et al., *Observation of Gravitational Waves from a Binary Black Hole Merger*, Phys. Rev. Lett. **116** (2016), no. 6, 061102, 1602.03837.

[6] Planck, P. A. R. Ade et al., *Planck 2015 results. XIII. Cosmological parameters*, Astron. Astrophys. **594** (2016), A13, 1502.01589.

[7] ATLAS, G. Aad et al., *Observation of a new particle in the search for the Standard Model Higgs boson with the ATLAS detector at the LHC*, Phys. Lett. **B716** (2012), 1–29, 1207.7214.

[8] CMS, S. Chatrchyan et al., *Observation of a new boson at a mass of 125 GeV with the CMS experiment at the LHC*, Phys. Lett. **B716** (2012), 30–61, 1207.7235.

[9] D. S. Salopek, J. R. Bond, and J. M. Bardeen, *Designing Density Fluctuation Spectra in Inflation*, Phys. Rev. **D40** (1989), 1753.

[10] F. L. Bezrukov and M. Shaposhnikov, *The Standard Model Higgs boson as the inflaton*, Phys. Lett. **B659** (2008), 703–706, 0710.3755.

[11] Planck, P. A. R. Ade et al., *Planck 2015 results. XX. Constraints on inflation*, Astron. Astrophys. **594** (2016), A20, 1502.02114.

[12] N. Makino and M. Sasaki, *The Density perturbation in the chaotic inflation with nonminimal coupling*, Prog. Theor. Phys. **86** (1991), 103–118.

[13] D. P. George, S. Mooij, and M. Postma, *Quantum corrections in Higgs inflation: the real scalar case*, JCAP **1402** (2014), 024, 1310.2157.

[14] M. Postma and M. Volponi, *Equivalence of the Einstein and Jordan frames*, Phys. Rev. **D90** (2014), no. 10, 103516, 1407.6874.

[15] A. Yu. Kamenshchik and C. F. Steinwachs, *Question of quantum equivalence between Jordan frame and Einstein frame*, Phys. Rev. **D91** (2015), no. 8, 084033, 1408.5769.

[16] G. Domènech and M. Sasaki, *Conformal Frame Dependence of Inflation*, JCAP **1504** (2015), no. 04, 022, 1501.07699.

[17] K. Kannike, G. Hutsi, L. Pizza, A. Racioppi, M. Raidal, A. Salvio, and A. Strumia, *Dynamically Induced Planck Scale and Inflation*, JHEP **05** (2015), 065, 1502.01334.

[18] D. P. George, S. Mooij, and M. Postma, *Quantum corrections in Higgs inflation: the Standard Model case*, JCAP **1604** (2016), no. 04, 006, 1508.04660.

[19] G. Domènech and M. Sasaki, *Conformal frames in cosmology*, Int. J. Mod. Phys. **D25** (2016), 1645006, 1602.06332.

[20] F. L. Bezrukov, A. Magnin, and M. Shaposhnikov, *Standard Model Higgs boson mass from inflation*, Phys. Lett. **B675** (2009), 88–92, 0812.4950.

[21] F. Bezrukov and M. Shaposhnikov, *Standard Model Higgs boson mass from inflation: Two loop analysis*, JHEP **07** (2009), 089, 0904.1537.

[22] K. Allison, *Higgs xi-inflation for the 125-126 GeV Higgs: a two-loop analysis*, JHEP **02** (2014), 040, 1306.6931.

[23] Y. Hamada, H. Kawai, K.-y. Oda, and S. C. Park, *Higgs Inflation is Still Alive after the Results from BICEP2*, Phys. Rev. Lett. **112** (2014), no. 24, 241301, 1403.5043.

[24] Y. Hamada, H. Kawai, K.-y. Oda, and S. C. Park, *Higgs inflation from Standard Model criticality*, Phys. Rev. **D91** (2015), 053008, 1408.4864.

[25] ATLAS, CMS, G. Aad et al., *Combined Measurement of the Higgs Boson Mass in pp Collisions at $\sqrt{s} = 7$ and 8 TeV with the ATLAS and CMS Experiments*, Phys. Rev. Lett. **114** (2015), 191803, 1503.07589.

[26] M. Holthausen, K. S. Lim, and M. Lindner, *Planck scale Boundary Conditions and the Higgs Mass*, JHEP **1202** (2012), 037, 1112.2415.

[27] F. Bezrukov, M. Y. Kalmykov, B. A. Kniehl, and M. Shaposhnikov, *Higgs Boson Mass and New Physics*, JHEP **1210** (2012), 140, 1205.2893.

[28] G. Degrassi, S. Di Vita, J. Elias-Miro, J. R. Espinosa, G. F. Giudice, et al., *Higgs mass and vacuum stability in the Standard Model at NNLO*, JHEP **1208** (2012), 098, 1205.6497.

[29] S. Alekhin, A. Djouadi, and S. Moch, *The top quark and Higgs boson masses and the stability of the electroweak vacuum*, Phys.Lett. **B716** (2012), 214–219, 1207.0980.

[30] I. Masina, *The Higgs boson and Top quark masses as tests of Electroweak Vacuum Stability*, Phys.Rev. **D87** (2013), 053001, 1209.0393.

[31] Y. Hamada, H. Kawai, and K.-y. Oda, *Bare Higgs mass at Planck scale*, Phys. Rev. **D87** (2013), no. 5, 053009, 1210.2538, [Erratum: Phys. Rev.D89,no.5,059901(2014)].

[32] F. Jegerlehner, *The Standard model as a low-energy effective theory: what is triggering the Higgs mechanism?*, Acta Phys. Polon. **B45** (2014), no. 6, 1167, 1304.7813.

[33] D. Buttazzo, G. Degrassi, P. P. Giardino, G. F. Giudice, F. Sala, A. Salvio, and A. Strumia, *Investigating the near-criticality of the Higgs boson*, JHEP **12** (2013), 089, 1307.3536.

[34] V. Branchina and E. Messina, *Stability, Higgs Boson Mass and New Physics*, Phys.Rev.Lett. **111** (2013), 241801, 1307.5193.

[35] A. Kobakhidze and A. Spencer-Smith, *The Higgs vacuum is unstable*, (2014), 1404.4709.

[36] A. Spencer-Smith, *Higgs Vacuum Stability in a Mass-Dependent Renormalisation Scheme*, (2014), 1405.1975.

[37] V. Branchina, E. Messina, and A. Platania, *Top mass determination, Higgs inflation, and vacuum stability*, JHEP **09** (2014), 182, 1407.4112.

[38] A. V. Bednyakov, B. A. Kniehl, A. F. Pikelner, and O. L. Veretin, *Stability of the Electroweak Vacuum: Gauge Independence and Advanced Precision*, Phys. Rev. Lett. **115** (2015), no. 20, 201802, 1507.08833.

[39] C. D. Froggatt and H. B. Nielsen, *Standard model criticality prediction: Top mass 173 +- 5-GeV and Higgs mass 135 +- 9-GeV*, Phys. Lett. **B368** (1996), 96–102, hep-ph/9511371.

[40] D. L. Bennett, *Multiple point criticality, nonlocality, and fine tuning in fundamental physics: Predictions for gauge coupling constants gives alpha**-1 = 136.8 +- 9*, Ph.D. thesis, Bohr Inst., 1996.

[41] C. Froggatt, H. B. Nielsen, and Y. Takanishi, *Standard model Higgs boson mass from borderline metastability of the vacuum*, Phys.Rev. **D64** (2001), 113014, hep-ph/0104161.

[42] H. B. Nielsen, *PREdicted the Higgs Mass*, Bled Workshops Phys. **13** (2012), no. 2, 94–126, 1212.5716.

[43] J. L. Cook, L. M. Krauss, A. J. Long, and S. Sabharwal, *Is Higgs Inflation Dead?*, Phys.Rev. **D89** (2014), 103525, 1403.4971.

[44] F. Bezrukov and M. Shaposhnikov, *Higgs inflation at the critical point*, Phys. Lett. **B734** (2014), 249–254, 1403.6078.

[45] D. Baumann, *Inflation*, in *Physics of the large and the small, TASI 09, proceedings of the Theoretical Advanced Study Institute in Elementary Particle Physics, Boulder, Colorado, USA, 1-26 June 2009*, 2011, pp. 523–686.

[46] Y. Nakanishi, *Regularization and conformal transformations of the power spectrum in general single field inflation*, masters' thesis, Osaka U., Inst. Phys., 2015.

[47] E. R. Harrison, *Fluctuations at the threshold of classical cosmology*, Phys. Rev. D **1** (1970), 2726–2730.

[48] Ya. B. Zeldovich, *A Hypothesis, unifying the structure and the entropy of the universe*, Mon. Not. Roy. Astron. Soc. **160** (1972), 1P–3P.

[49] A. L. Alinea, T. Kubota, Y. Nakanishi, and W. Naylor, *Adiabatic regularisation of power spectra in k-inflation*, JCAP **1506** (2015), no. 06, 019, 1503.08073.

[50] S. C. Park and S. Yamaguchi, *Inflation by non-minimal coupling*, JCAP **0808** (2008), 009, 0801.1722.

[51] Y. Hamada, H. Kawai, Y. Nakanishi, and K.-y. Oda, *Meaning of the field dependence of the renormalization scale in Higgs inflation*, Phys. Rev. **D95** (2017), no. 10, 103524, 1610.05885.

[52] M. Shaposhnikov and D. Zenhausern, *Scale invariance, unimodular gravity and dark energy*, Phys. Lett. **B671** (2009), 187–192, 0809.3395.

[53] M. Shaposhnikov and D. Zenhausern, *Quantum scale invariance, cosmological constant and hierarchy problem*, Phys. Lett. **B671** (2009), 162–166, 0809.3406.

[54] M. E. Shaposhnikov and I. I. Tkachev, *Quantum scale invariance on the lattice*, Phys. Lett. **B675** (2009), 403–406, 0811.1967.

[55] K. Nakayama and F. Takahashi, *Higgs Chaotic Inflation and the Primordial B-mode Polarization Discovered by BICEP2*, Phys. Lett. **B734** (2014), 96–99, 1403.4132.

[56] P. Minkowski, $\mu \to e\gamma$ *at a Rate of One Out of* 10^9 *Muon Decays?*, Phys. Lett. **67B** (1977), 421–428.

[57] T. Yanagida, in *Proceedings of the Workshop on Unified Theory and Baryon Number of the Universe*, edited by O. Sawada and A. Sugamoto (KEK, Tokyo, 1979), p. 95; M. Gell-Mann, P. Ramond, and R. Slanski, in *Supergravity*, edited by P. van Nieuwenhuizen and D. Freedman (North-Holland, Amsterdam, 1979) arXiv:1306.4669; S. L. Glashow, in *Proceedings of the Cargése Summer Institute on Quarks and Leptons*, Cargése, July 9–29, 1979, eds. M. Lévy et al. (Plenum, 1980, New York), p. 707; R. N. Mohapatra and G. Senjanovic, *Neutrino Mass and Spontaneous Parity Violation*, Phys. Rev. Lett. **44** (1980) 912.

[58] Y. Hamada, H. Kawai, Y. Nakanishi, and K.-y. Oda, *Higgs inflation puts lower and upper bounds on tensor-to-scalar ratio and on Higgs-portal-dark-matter mass*, (2017), 1709.09350.

[59] Y. Hamada, H. Kawai, and K.-y. Oda, *Minimal Higgs inflation*, PTEP **2014** (2014), 023B02, 1308.6651.

[60] C. P. Burgess, H. M. Lee, and M. Trott, *Power-counting and the Validity of the Classical Approximation During Inflation*, JHEP **09** (2009), 103, 0902.4465.

[61] J. L. F. Barbon and J. R. Espinosa, *On the Naturalness of Higgs Inflation*, Phys. Rev. **D79** (2009), 081302, 0903.0355.

[62] C. P. Burgess, H. M. Lee, and M. Trott, *Comment on Higgs Inflation and Naturalness*, JHEP **07** (2010), 007, 1002.2730.

[63] M. P. Hertzberg, *On Inflation with Non-minimal Coupling*, JHEP **11** (2010), 023, 1002.2995.

[64] A. Salvio and A. Mazumdar, *Classical and Quantum Initial Conditions for Higgs Inflation*, Phys. Lett. **B750** (2015), 194–200, 1506.07520.

[65] Y. Ema, R. Jinno, K. Mukaida, and K. Nakayama, *Violent Preheating in Inflation with Nonminimal Coupling*, JCAP **1702** (2017), no. 02, 045, 1609.05209.

[66] Y. Hamada, H. Kawai, and K.-y. Oda, *Eternal Higgs inflation and the cosmological constant problem*, Phys. Rev. **D92** (2015), 045009, 1501.04455.

[67] J. M. Cline, K. Kainulainen, P. Scott, and C. Weniger, *Update on scalar singlet dark matter*, Phys. Rev. **D88** (2013), 055025, 1306.4710, [Erratum: Phys. Rev.D92,no.3,039906(2015)].

[68] Y. Hamada, H. Kawai, and K.-y. Oda, *Predictions on mass of Higgs portal scalar dark matter from Higgs inflation and flat potential*, JHEP **1407** (2014), 026, 1404.6141.

[69] XENON, E. Aprile et al., *First Dark Matter Search Results from the XENON1T Experiment*, Phys. Rev. Lett. **119** (2017), no. 18, 181301, 1705.06655.

[70] PandaX-II, X. Cui et al., *Dark Matter Results From 54-Ton-Day Exposure of PandaX-II Experiment*, Phys. Rev. Lett. **119** (2017), no. 18, 181302, 1708.06917.

[71] LUX, D. S. Akerib et al., *Results from a search for dark matter in the complete LUX exposure*, Phys. Rev. Lett. **118** (2017), no. 2, 021303, 1608.07648.

[72] Particle Data Group, C. Patrignani et al., *Review of Particle Physics*, Chin. Phys. **C40** (2016), no. 10, 100001.

[73] G. Cortiana, *Top-quark mass measurements: review and perspectives*, Rev. Phys. **1** (2016), 60–76, 1510.04483.

[74] POLARBEAR, Y. Inoue et al., *POLARBEAR-2: an instrument for CMB polarization measurements*, Proc. SPIE Int. Soc. Opt. Eng. **9914** (2016), 99141I, 1608.03025.

[75] T. Matsumura et al., *Mission design of LiteBIRD*, (2013), 1311.2847, [J. Low. Temp. Phys.176,733(2014)].

[76] CORE, J. Delabrouille et al., *Exploring Cosmic Origins with CORE: Survey requirements and mission design*, (2017), 1706.04516.

[77] Super-Kamiokande, Y. Fukuda et al., *Evidence for oscillation of atmospheric neutrinos*, Phys. Rev. Lett. **81** (1998), 1562–1567, hep-ex/9807003.

[78] SNO, Q. R. Ahmad et al., *Direct evidence for neutrino flavor transformation from neutral current interactions in the Sudbury Neutrino Observatory*, Phys. Rev. Lett. **89** (2002), 011301, nucl-ex/0204008.

[79] F. Capozzi, E. Di Valentino, E. Lisi, A. Marrone, A. Melchiorri, and A. Palazzo, *Global constraints on absolute neutrino masses and their ordering*, Phys. Rev. **D95** (2017), no. 9, 096014, 1703.04471.

[80] CMS Collaboration, *Updates on Projections of Physics Reach with the Upgraded CMS Detector for High Luminosity LHC*, (2016), https://cds.cern.ch/record/2221747.

[81] N. Haba, H. Ishida, and R. Takahashi, *Higgs inflation and Higgs portal dark matter with right-handed neutrinos*, PTEP **2015** (2015), no. 5, 053B01, 1405.5738.

[82] K. Kawana, *Multiple Point Principle of the Standard Model with Scalar Singlet Dark Matter and Right Handed Neutrinos*, PTEP **2015** (2015), 023B04, 1411.2097.